Nephrol Dial Transplant (2023) 38: 322–343
https://doi.org/10.1093/ndt/gfac220
Advance Access publication date 22 July 2022

ORIGINAL ARTICLE

The direct effect of fibroblast growth factor 23 on vascular smooth muscle cell phenotype and function

Noemi Vergara[1,2,*], M. Victoria Pendón-Ruiz de Mier[1,2,3,4,*], Cristian Rodelo-Haad[1,2,3,4,*], Gonzalo Revilla-González[5], Cristina Membrives[1,2], Juan M. Díaz-Tocados[1,2], Julio M. Martínez-Moreno[1,2], Ana I. Torralbo[1,2], Carmen Herencia[1,2], María Encarnación Rodríguez-Ortiz[1,2], Rodrigo López-Baltanás[1,2], Williams G. Richards[6], Arnold Felsenfeld[7], Yolanda Almadén[1,8,9], Alejandro Martin-Malo[1,2,3,4], Juan Ureña[5], Rafael Santamaría[1,3,4], Sagrario Soriano[1,2,3,4], Mariano Rodríguez[1,2,3,4,†] and Juan R. Muñoz-Castañeda[1,2,3,4,†]

[1]Maimonides Institute for Biomedical Research of Cordoba, Cordoba, Spain, [2]University of Cordoba, Spain, [3]Nephrology Service, Reina Sofia University Hospital, Cordoba, Spain, [4]Spanish Renal Research Network (REDinREN), Institute of Health Carlos III, Madrid, Spain, and the European Uremic Toxins group, [5]Instituto de Biomedicina de Sevilla, Hospital Universitario Virgen del Rocío/CSIC/Universidad de Sevilla, Departemento de Fisiología Médica y Biofísica, Sevilla, Spain, [6]Amgen Inc., Thousand Oaks, CA, USA, [7]Department of Medicine, Veterans Affairs Greater Los Angeles Healthcare System and the David Geffen School of Medicine, University of California, Los Angeles, CA, USA, [8]Internal Medicine Service, Reina Sofia University Hospital, Cordoba, Spain and [9]Spanish Biomedical Research Networking Centre consortium for the area of Physiopathology of Obesity and Nutrition, Institute of Health Carlos III, Madrid, Spain

*These authors contributed equally to this work.
†These authors share the last authorship.
Correspondence to: Juan R. Muñoz-Castañeda; E-mail: juanr.munoz.exts@juntadeandalucia.es; Rafael Santamaría; E-mail: rsantamariao@gmail.com

ABSTRACT

Background. In chronic kidney disease (CKD) patients, increased levels of fibroblast growth factor 23 (FGF23) are associated with cardiovascular mortality. The relationship between FGF23 and heart hypertrophy has been documented, however, it is not known whether FGF23 has an effect on vasculature. Vascular smooth muscle cells VSMCs may exhibit different phenotypes; our hypothesis is that FGF23 favours a switch from a contractile to synthetic phenotype that may cause vascular dysfunction. Our objective was to determine whether FGF23 may directly control a change in VSMC phenotype.

Methods. This study includes *in vitro*, *in vivo* and *ex vivo* experiments and evaluation of patients with CKD stages 2–3 studying a relationship between FGF23 and vascular dysfunction.

Results. *In vitro* studies show that high levels of FGF23, by acting on its specific receptor FGFR1 and Erk1/2, causes a change in the phenotype of VSMCs from contractile to synthetic. This change is mediated by a downregulation of *miR-221/222*, which augments the expression of MAP3K2 and PAK1. *miR-221/222* transfections recovered the contractile phenotype of VSMCs. Infusion of recombinant FGF23 to rats increased vascular wall thickness, with VSMCs showing a synthetic phenotype with a reduction of *miR-221* expression. *Ex-vivo* studies on aortic rings demonstrate also that high FGF23 increases arterial stiffening. In CKD 2–3 patients, elevation of FGF23 was associated with increased pulse wave velocity and reduced plasma levels of *miR-221/222*.

Conclusion. In VSMCs, high levels of FGF23, through the downregulation of *miR-221/222*, causes a change to a synthetic phenotype. This change in VSMCs increases arterial stiffening and impairs vascular function, which might ultimately worsen cardiovascular disease.

Keywords: arterial stiffness, chronic kidney disease, FGF23, microRNA, vascular smooth muscle cells

GRAPHICAL ABSTRACT

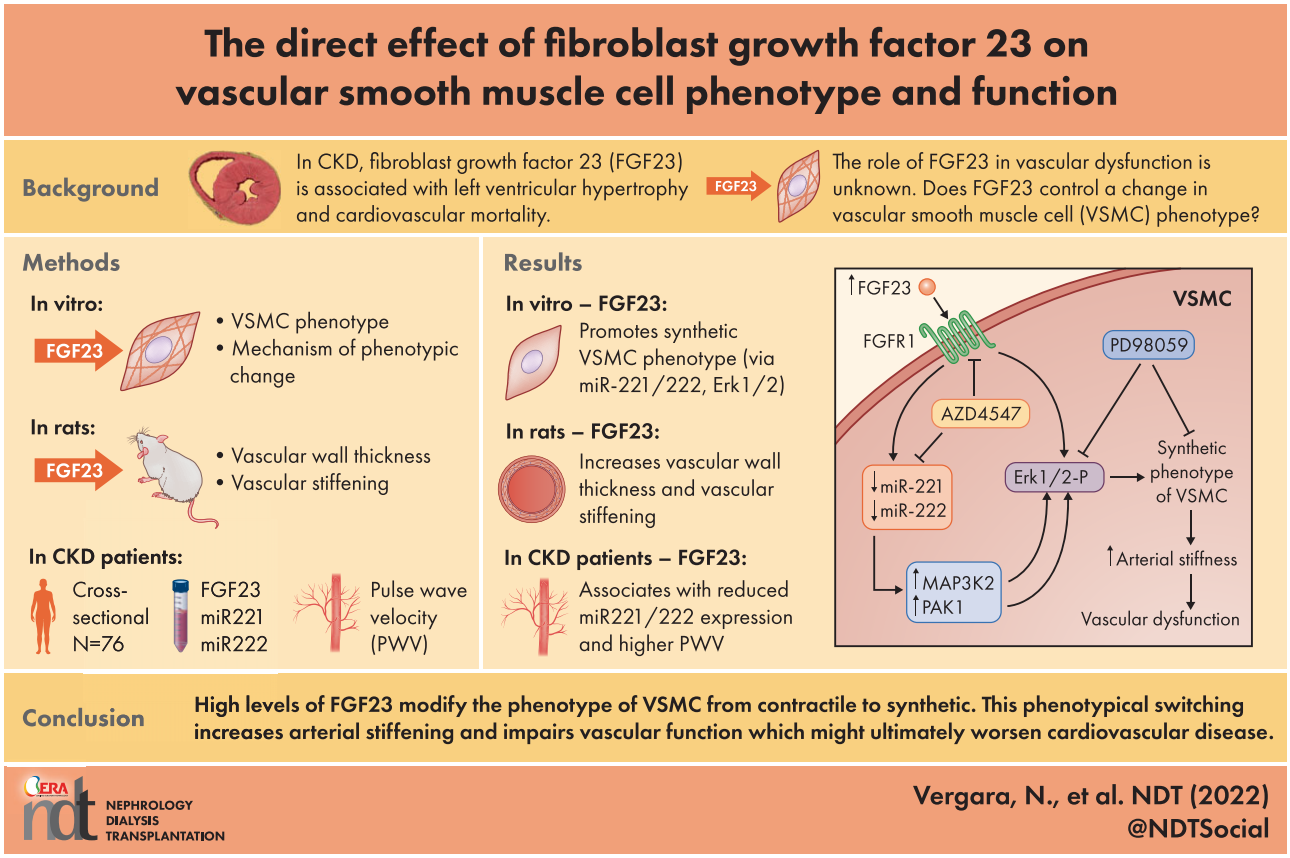

KEY LEARNING POINTS

What is already known about this subject?

- Serum concentration of FGF23 is increased in patients with chronic kidney disease and this is associated with left ventricular hypertrophy and cardiovascular mortality.
- Similarly, a potential relationship between high levels of FGF23 and endothelial damage has been also described.

What this study adds?

- In human aorta vascular smooth muscle cells, high levels of FGF23 promote a switch from a contractile to a synthetic phenotype.
- This effect is mediated by downregulation of *miR-221/222* and FGFR1 and Erk1/2 phosphorylation.
- *In vivo*, high levels of FGF23 induce changes of VSMC morphology, increasing arterial wall thickness and arterial stiffening.
- The effect of FGF23 on the VSMC phenotype is not affected by Klotho administration.
- In CKD stage 2–3 patients with high levels of FGF23, there is decreased expression of *miR-221/222* and there is a correlation between FGF23 levels and pulse wave velocity.

What impact this may have on practice or policy?

- The effects of high levels of FGF23 on VSMCs further explain the association between FGF23 and cardiovascular mortality.
- In the early stages of CKD, an increase in FGF23 should be prevented to reduce cardiovascular damage.
- A reduction in phosphate in the diet could decrease FGF23, preventing arterial remodelling and vascular dysfunction.

INTRODUCTION

Fibroblast growth factor 23 (FGF23) is a bone-derived hormone that produces phosphaturia, reduces vitamin D levels [1] and inhibits the synthesis and secretion of parathyroid hormone [2]. The serum concentration of FGF23 is elevated in patients with early stages of chronic kidney disease (CKD) and increases progressively with the decline of renal function [3]. In CKD patients and in the general population (although with lower levels of FGF23 than in CKD), high serum concentrations of FGF23 are associated with cardiovascular mortality [4]; it has been shown that FGF23 induces myocardial cell proliferation and left ventricular hypertrophy

[5, 6]. It is not known whether FGF23 has a direct effect on the vascular wall, particularly vascular smooth muscle cells (VSMCs). Certainly, the strong association between FGF23 and cardiovascular mortality [4] could be supported by the cardiac effects of FGF23; however, this does not rule out involvement of the vasculature. With respect to endothelial cells, it has been reported that FGF23 causes endothelial dysfunction [7, 8].

The VSMCs exhibit two functional phenotypes, contractile and synthetic, which correspond to the two ends of a wide spectrum of intermediate phenotypes; these phenotypes confer a specific function and a distinct morphology [9]. In a healthy vascular wall, the normal activity of VSMCs includes an adequate change in the phenotype as part of the process of wall renewal and repair of tissue damage induced by small injuries [10]. If this VSMC plasticity is extensively modified, it is expected that we would observe vascular dysfunction. The balance between contractile and synthetic VSMC phenotypes is tightly regulated since it plays an important role in vascular function [11]. Switching of the VSMC phenotype from contractile to synthetic has been linked to diseases affecting the vascular wall, such as hypertension and atherosclerosis [12]. The synthetic phenotype of VSMCs is characterized by increased cell proliferation and migration, a decreased number of fusiform cells, increased production of extracellular proteins, decreased expression of elastin [13, 14] or myosin heavy chain [15]; the end result is an increase in arterial stiffening [16].

Recent studies have shown that alteration of VSMC microRNA (miRNA) expression may be responsible for some abnormalities observed in diseased vessels [17]. In the present study we also considered the possibility that FGF23 could have an effect on the VSMC phenotype through changes in miRNA expression. *miR-221* and *miR-222* are highly expressed in VSMCs and endothelial cells [18]; the expression of *miR-221/222* is closely linked to preservation of the contractile phenotype of VSMCs from the pulmonary artery [18–20]. A potential relationship between FGF23, aortic VSMC miRNA and arterial stiffening has not been fully explored.

Our hypothesis is that high levels of FGF23 have a direct effect on the VSMC phenotype, which may contribute to the development of vascular dysfunction and cardiovascular disease. In CKD patients, the effort to reduce FGF23 levels to decrease cardiovascular mortality will be even more justified if indeed there is evidence that FGF23 directly affects the vasculature. Therefore the objective of this study was to evaluate the effect of high FGF23 levels on the VSMC phenotype and vascular function as well as to investigate the potential mechanisms involved.

MATERIALS AND METHODS

The data obtained in this study are available from the corresponding author upon reasonable request.

VSMC culture

Human aortic VSMCs from the same male donor were obtained from Clonetics (Lonza, Walkersville, MD, USA). Cells were cultured in Dulbecco's Modified Eagle Medium (DMEM) supplemented with heat-inactivated Hyclone (South Logan, Utah, USA) foetal bovine serum (20%), sodium pyruvate (1 mM; Lonza), glutamine (4.5 g/l; Lonza, Verviers, Belgium), penicillin (100 U/ml; Laboratorios ERN, Barcelona, Spain), streptomycin (100 mg/ml; Laboratorios Normon, Madrid, Spain), fungizone and HEPES (20 mM; Sigma-Aldrich, St. Louis, MO, USA) at 37°C in a humidified atmosphere with 5% carbon dioxide. VSMCs in passages 2–6 were used for these experiments.

In control groups, VSMCs were cultured with DMEM for 9 days with a change of culture medium and treatments every 48 h. Treated cells were incubated in the medium described above with the addition of two concentrations of human recombinant FGF23 (rFGF23; 2 or 20 ng/ml (kindly donated by Amgen, Thousand Oaks, CA, USA). In addition, depending on the experiments, cells were cultured with either AZD4547 (150 nM), a selective FGF receptor (FGFR) inhibitor targeting FGFR1/2/3 (Selleckchem, Houston, TX, USA) or with PD98059 (10 μM; Sigma-Aldrich), an inhibitor of the MEK/ERK pathway.

Other experiments were performed to determine if the effects of FGF23 are or are not dependent on klotho. Human recombinant klotho (KL1 and KL2; R&D Systems, Minneapolis, MN, USA) was added in a concentration of 20 ng/ml to VSMCs treated with FGF23 (2 ng/ml) for 9 days and the expression of elastin and myosin heavy chain (MHC) mRNA were evaluated.

Cell proliferation assay

VSMCs were seeded in 96-well plates and rFGF23 (2 and 20 ng/ml) was added for 24 hours. Reagent WST-1 was used to evaluate cell proliferation (Roche Diagnostics, Basel, Switzerland).

Analysis of changes in mRNA expression by reverse transcription polymerase chain reaction (RT-PCR)

Total RNA was isolated from cultured VSMCs using 1 ml Tri-Reagent (Sigma-Aldrich) and it was quantified by spectrophotometry (ND-1000; Nanodrop Technologies, Wilmington, DE, USA). VSMC markers, elastin and MHC were measured by real-time quantitative RT-PCR (qRT-PCR; LC480; Roche Diagnostics) and the SensiFast SYBR No-ROX One-Step Kit (Bioline, London, UK) in a final volume of 10 μL from 50 ng of total RNA. The expression of target genes was normalized to the expression of *glyceraldehyde-3-phosphate* dehydrogenase (GAPDH). The human primers for RT-PCR amplification are shown in Table 1.

The effect of FGF23 on the miRNA profile

To evaluate a potential effect of FGF23 on the miRNA profile, the Human Cardiovascular Disease miScript miRNA PCR Array from Qiagen (Valencia, CA, USA) was used. This array examines the expression of 84 miRNAs known to exhibit altered expression in cardiovascular diseases, allowing the evaluation of the most relevant miRNAs, some of them involved in arterial stiffening and vascular remodelling. Using

Table 1. Human and rat primer sequences used for RT-PCR

Gene name	Forward	Reverse
Human *Elastin*	5′GCTCTGCACCTGTTCCTC3′	5′CTGCGTCTTCCACACCAC3′
Human *MHC*	5′CGAGCTCTCCGTCATCTTG3′	5′GCTGAATGACAACGTGACTTC3′
Human *MAP3K2*	5′TGTGTGTGTGTGTGGTTAGAG3′	5′GGAAGGTGAGTATGGGAAGAT3′
Human *AGO1*	5′GCGTAGCCATTCCCAAGA3′	5′GCAGCTCATTATTGTCATCCT3′
Human *AGO2*	5′ACCTTGAAGATGCGATCCTTG3′	5′AGAATCTATACACAGCCATGCC3′
Human *Exportin 5*	5′TGGCCACAGAGGTCACCCCC3′	5′GGGGCGCAGTGCCTCGTAT3′
Human *Drosha*	5′ACCGTTACTTCTCGTCTCATTG3′	5′GCCACCTCCTAGCAAATAGTC3′
Human *GAPDH*	5′TGATGACATCAAGAAGGTGGTGAAG3′	5′TCCTTGGAGGCCATGTGGGCCAT3′
Rat *MHC*	5′GAGAATGAGAAGAAAGCCAAGAG3′	5′CATCCAGCTCCCGCTGCAGCT3′
Rat *Elastin*	5′CAGCTAAAGCAGCGAAGTATG3′	5′CCTGTAATGCCTCCAATCCC3′
Rat *GAPDH*	5′CATGGAGAAGGCTGGGGCTCA3′	5′GTGATGGCATGGACTGTGGTCAT3′
miRNA sequences		
miR-221-3p	5′AGCUACAUUGUCUGCUGGGUUUC3′	
miR-222-3p	5′AGCUACAUCUGGCUACUGGGU3′	
miR-26a-5p	5′ UUCAAGUAAUCCAGGAUAGGCU3′	
miR-145-5p	5′GUCCAGUUUUCCCAGGAAUCCCU3′	

SYBR Green real-time PCR and U6 for housekeeping, a relative quantification through the $2^{-\Delta Ct}$ method was performed.

Following the manufacturer's instructions, two M96 plates were used, including pooled samples from the control culture or FGF23-treated VSMCs for 9 days.

Thereafter, the expression of some altered miRNAs, including *miR-221*, *miR-222*, *miR-26a* and *miR-145*, was validated by RT-PCR. Total RNA was isolated from each sample using 1 ml Tri-Reagent (Sigma-Aldrich). Complementary DNA (cDNA) was synthesized from 10 ng of each sample using the miRCURY LNA Universal RT microRNA PCR system (Qiagen) according to manufacturer's instructions. miRNA expression was measured by SYBR green GoTaq qPCR Master Mix (Promega, Madison, WI, USA). The target sequence of the LNA PCR primers for these miRNAs is shown in Table 1. The $2^{-\Delta Ct}$ method was used to calculate the relative abundance of miRNAs compared with miR-U6 endogenous control expression.

The expression of specific genes related to miRNA biogenesis such as *argonaute 1* (*AGO1*), *argonaute 2* (*AGO2*), *exportin 5* and *Drosha* (Table 1) was also determined by RT-PCR.

Cell transfection of *miR-221*, *miR-222*, anti-*miR-221* and anti-*miR-222*

To upregulate *miR-221* and *miR-222*, FGF23-treated VSMCs with 2 ng/ml rFGF23 for 9 days were transfected with *miR-221* and *miR-222* using a complete medium without antibiotics (Opti-MEM, Life Technologies, Madrid, Spain). Cell transfection was achieved by addition of 100 nmol/L miRNA mimic (Life Technologies) for *miR-221-3p*, *miR-222-3p* or non-specific control (scrambled) by using siPORT NeoFX transfection agent (Life Technologies) according to the manufacturer's instructions.

Anti-*miR-221* and anti-*miR-222* were also transfected to confluent VSMCs for 48 hours using the same protocol described above. After 48 hours, total RNA was isolated and cDNA and qPCR were performed as indicated in the previous section using endogenous miR-U6 as a control. In these conditions, we compared the expressions of elastin and *miR-221/222*.

Protein extracts and western blot

Cytosolic proteins were isolated from VSMCs in a lysis buffer containing 10 mM HEPES, 10 mM KCl, 0.1 mM EDTA, 0.1 mM EGTA, 1 mM DTT, 0.5 mM PMSF, 70 μg/ml protease inhibitor cocktail and 0.5% Igepal CA-630, pH 7.9. The suspensions were centrifuged and the supernatants (cytosolic extracts) were stored. Nuclear extracts were obtained by incubating the pellet separated from the cytosolic extract in a lysis buffer containing 20 mM HEPES, 0.4 mM NaCl, 1 mM EDTA, 1 mM EGTA, 1 mM dithiothreitol, 1 mM PMSF and 46 µg/ml protease inhibitor cocktail at pH 7.9. The protein concentration was determined with the Bradford method (Bio-Rad Laboratories, Munich, Germany). For western blot, equal amounts of protein were electrophoresed in 4–20% sodium dodecyl sulphate–polyacrylamide gradient gel (Bio-Rad Laboratories). The proteins were subsequently transferred to a nitrocellulose membrane (Bio-Rad Laboratories). The membranes were blocked with either 5% milk or 5% bovine serum albumin (BSA) for 1 hour at room temperature and then incubated with primary antibody overnight at 4°C. The primary antibodies used included rabbit monoclonal cyclin D1 (D1:1000; Cell Signaling Technology, Danvers, MA, USA), mouse monoclonal proliferating cell nuclear antigen (PCNA; 1 μg/ml; Santa Cruz Biotechnology, Dallas, TX, USA), rabbit polyclonal elastin (5 μg/ml; GeneTex, Irvine, CA, USA), mouse matrix metallopeptidase 9 (MMP9; D1:500; Santa Cruz Biotechnology), rabbit polyclonal FGFR1p (Tyr 653, Tyr 654; D1:200; Thermo Fisher Scientific, Madrid, Spain), rabbit polyclonal FGFR1 (5 μg/ml; Sigma-Aldrich), rabbit monoclonal phospho-p44/42 MAPK (Erk1/2; Tyr202/Tyr204; D1:2000; Cell Signaling Technology), rabbit monoclonal p44/42 MAPK (Erk1/2; D1:1000; Cell Signaling Technology), mouse monoclonal MAP3K2 (D1:1000; Abcam, Cambridge, UK), mouse monoclonal tubulin (1 μg/ml; Abcam) and mouse monoclonal TFIIB (D1:1000; Cell Signaling Technology). Tubulin and TFIIB protein were used as cytoplasmic and nuclear loading controls, respectively. Blots were immunolabeled using either a rabbit or a mouse horseradish peroxidase–conjugated secondary antibody (D1:5000; Santa Cruz Biotechnology) and developed on autoradiographic film using the ECL Western

Blotting Detection System (Amersham Biosciences, Little Chalfont, UK) in LAS 4000 (GE Healthcare Life Science, Boston, USA).

Confocal microscopy

VSMCs were seeded on coverslips and received 0, 2 or 20 ng/ml of FGF23 for 9 days. Then they were rinsed in phosphate-buffered saline (PBS), fixed and permeated in cold 50% methanol for 2 min, cold 100% methanol for 20 min and cold 50% methanol for 2 min. The specimens were subsequently washed at room temperature in PBS (3 × 5 min) and incubated for 2 hours with smooth muscle actin (SMA; fluorescein isothiocyanate, 20 μg/ml; GeneTex, Irvine, CA, USA) in blocking solution (1% BSA) at room temperature. After being washed with PBS (3 × 5 min), the specimens were counterstained with 4′,6-diamino-2-phenylindole dihydrochloride (DAPI, Invitrogen, Paisley, UK) for nuclear stain. Pictures were obtained at 40× using an inverted confocal microscope (LSM5 Exciter, Zeiss, Oberkochen, Germany). ImageJ software was used to quantify the intensity of fluorescence and to analyse cell and nucleus length:width ratios of the cells visualized by confocal microscopy.

Experiments in animal models

All experiments were performed in rats and the protocols were reviewed and approved by the Local Ethics Committee for Animal Research of the University of Cordoba. All rats received humane care in compliance with the guidelines from Directive 2010/63/EU of the European Parliament on the protection of animals used for scientific purposes (UCO1745).

Experimental design. Eight-week-old male Wistar rats, weight 250–300 g, from Charles River Laboratories (Barcelona, Spain) were used. Male rats were chosen because oestradiol has been demonstrated to affect the synthetic phenotype of VSMCs [21]. All animals were housed in individual cages in the same room. Animals were separated into a control group that received vehicle (buffer A5Su pH 5.2, $n = 5$) and another group that received rat rFGF23 (donated by Amgen, $n = 6$). Rats were anesthetized using sevofluorane (Abbott, Madrid, Spain) and a mini-osmotic pump (Alzet model 2004 purchased from Charles River Laboratories, Barcelona, Spain) was implanted subcutaneously between the shoulders and loaded with either rFGF23 or vehicle. The rFGF23 was infused at 15 μ/day over 14 days as described previously [22]. A single dose of 75 mg/kg weight of buprenorphine was used for analgesia after Alzet pump implantation. To avoid rFGF23-induced hypophosphatemia, dietary phosphate was moderately increased to 0.9% in all rats. Likewise, to prevent a decline in calcitriol caused by FGF23, all rats received calcitriol supplementation (8 ng/rat, intraperitoneally three times per week).

Blood pressure (BP) measurements

Systolic, diastolic and mean bp were measured using a non-invasive tail cuff system (LE 5001 Pressure Meter, Harvard Apparatus, Panlab, Barcelona, Spain) in control and rFGF23 rats after the 14-day period of treatment. Pulse pressure (PP) was calculated as the difference between systolic and diastolic BP. A total of 8–10 measurements were obtained for each animal.

Collections of blood, urine and histological analysis of aortic tissue

Blood for biochemical determinations was obtained from the abdominal aorta at the time of sacrifice after anaesthesia using xylazine (5 mg/kg) and thiopental (50 mg/kg). Twenty-four-hour urine was collected in metabolic cages for measurement of phosphate excretion.

Haematoxylin and eosin staining of the thoracic aorta was performed using a commercial kit from Thermo Fisher Scientific. To evaluate extracellular matrix deposition, picrosirius staining of the aorta was also performed. Paraffin-embedded aorta was cut into 4-mm slices and stained with Sirius Red F3BA (0.5% in saturated aqueous picric acid; Sigma-Aldrich). Other studies [23] have shown that picrosirius staining can be visualized through confocal microscopy to evaluate structural changes. Aortas were excited at 633 nm using filters of 636–754 nm in a Zeiss LSM 710 laser scanning confocal microscope at the Maimonides Institute for Biomedical Research of Cordoba. Immunohistochemistry for elastin, fibronectin and MMP9 was also performed on thoracic aortas using the Novolink Polymer Detection System kit (Leica Biosystems, Newcastle, UK) according to the manufacturer's instructions. Anti-fibronectin (mouse fibronectin; D1:250; Santa Cruz Biotechnology), anti-MMP9 (D1:50; Santa Cruz Biotechnology) and anti-elastin (rabbit polyclonal elastin; 5 μg/ml; GeneTex) were used as the primary antibodies. Finally, PBS was used to perform a negative immunostaining to substrate background. Images were taken using a Leica DM2000 LED microscope with a Leica MC190 HD camera using Leica Application Suite 4.8.0 software (all from Leica Biosystems, Newcastle, UK). J software was used to analyse structural changes and immunohistochemistry quantification.

RNA isolation and qRT-PCR for miRNA expression in rat aorta

After 14 days of FGF23 infusion, abdominal aortas were collected to analyse changes in mRNA expression. Total RNA was isolated from each aorta section using 1 ml Tri-Reagent (Sigma-Aldrich). mRNA and qPCR were performed using the same protocol indicated above. *Elastin*, *MHC*, *miR-221-3p* and *miR-222-3p* mRNA levels were determined by real-time qRT-PCR (Light cycler, Roche Diagnostics). The rat primers for RT-PCR are indicated in Table 1.

Measurement of contractility in arterial rings

Rat thoracic aortas were cleaned of connective tissue, cut in rings (2 mm long and mounted on a wire myograph (610M model, Danish Myo Technology, Hinnerup, Denmark). Rings were placed in chambers filled with physiological

solution and bubbled with 95% oxygen and 5% carbon dioxide at pH 7.4. Arterial rings were initially normalized to measure passive wall tension, the force exerted by the vessel wall in the absence of smooth muscle activation. This was accomplished by feeding two wires through the vessel lumen; one wire was affixed to a sensitive force transducer to measure changes in wall tension and the other was attached to a micropositioner that allows precise control of the distance between the two wires. Intact vessel segments were successively stretched with 200-μm steps until transmural pressure reached 100 mmHg, then experiments were done at 90% of 100 mmHg transmural pressure for optimum records. These procedures were performed in accordance with the user manual provided by the manufacturer. Wall stress (σ, dyn/cm^2) and strain were determined from values of force (dyn), mass (g) and geometric arterial parameters (cm) [24]. Geometric arterial parameters were obtained from the following equations. The internal circumference (C) of the rings was determined from the gap distance (X) using the following equation:

$$C = 2X + \pi(R_1 + R_2),$$

where R_1 and R_2 are the radius of the two wires (cm) and X is the gap distance between the middles of the wires (cm). From the circumference, the equivalent internal radius of the ring (α) was obtained:

$$C = 2\pi\alpha.$$

Once α was obtained, the equivalent external radius (b) of the ring was also determined:

$$b^2 = \alpha^2 + \frac{W}{\pi\rho w},$$

where w is the width of the ring (cm), ρ is the density of the sample (1.06 g/cm^3) and W is the weight of the segment (g). Finally, assuming that an isovolumetric deformation occurred, thickness (h) was obtained from

$$h = b - a.$$

The value of circumferential wall stress (σ, dyn/cm^2) was determined from measured values of force (Y, dyn) given by the wire micrograph:

$$\sigma = \frac{Y}{2hw}.$$

Strain was calculated using the following relation:

$$Strain = \frac{\Delta C}{C_i}.$$

After normalization, arterial rings were stabilized for 1 hour and then active wall tension was measured. We used noradrenaline (3 μM) and high potassium solution (70K) to induce smooth muscle contraction via activation of alpha1-adrenoceptor and L-type Ca^{2+} channels, respectively. 70K solution was obtained by replacing 70 mM of NaCl with KCl in the extracellular solution. Noradrenaline and 70K were added directly to the chambers while vessel tension was monitored. Experiments were performed at 37°C.

Study in patients with CKD stage 2–3

This research protocol complies with the Declaration of Helsinki and was approved by the ethics committee of the Reina Sofia Hospital in Cordoba and written informed consent was obtained (EudraCT number 2015-000619-42).

The relationship between FGF23 levels, arterial stiffening and serum levels of *miR-221* and *miR-222* was analysed in a group of 76 patients with CKD stage 2–3 (glomerular filtration rate 30–90 ml/min/1.73 m^2) and clinical criteria of metabolic syndrome (defined according to the statement criteria from Alberti *et al.* [25]). Patients were included prospectively as they attended the outpatient clinic.

Baseline data are shown in Table 4. Brachial BP readings were taken three times in a seated position with a time interval of 1 min between successive measurements using an automated device to reduced the potential for observer biases. The arm was supported at heart level. The average of the three determinations was considered as the value of BP (systolic and diastolic BP, peripheral PP and heart rate). Central BP (systolic, diastolic and peripheral PP), cardiac output, cardiac index, peripheral vascular resistance and pulse wave velocity (PWV) were obtained with a Mobil-O-Graph (IEN, Aachen, Germany) [26].

Blood and urine samples were collected to evaluate biochemical parameters. Serum phosphate and creatinine were measured by spectrophotometry (Biosystems SA, Barcelona, Spain). Plasma levels of the C-terminal fragment of FGF23 (C-FGF23) were determined using an enzyme-linked immunosorbent assay kit (Immutopics, San Clemente, CA, USA).

RNA isolation and qRT-PCR for miRNA expression in plasma from rats and CKD patients

In rats, miRNA-221 and miRNA-222 were measured in plasma from five animals of the vehicle group and six from FGF23-treated animals.

In patients, the amount of miRNA-221 and miRNA-222 was measured in seven patients with the highest serum concentration of C-FGF23 (highest decile) and seven patients with the lowest levels of C-FGF23 (lowest decile). Total RNA, including the miRNA fraction, was isolated from a plasma sample of 200 μl using the QIAzol miRNeasy kit (Qiagen) according to the manufacturer's instructions. Due to the absence of an endogenous miRNA control in plasma, a non-human synthetic miRNA was added to each of the samples as an internal control (*C. elegans* miR-39 mimic: 5′-UCACCGGGUGUAAAUCAGCUUG-3′; Qiagen). Finally, the total RNA was eluted in 14 μl of RNAse-free water. cDNA was synthesized from 3 μL of each sample using miRCURY LNA Universal RT microRNA PCR system (Qiagen) according to manufacturer's instructions. The $2^{-\Delta Ct}$ method was used to calculate the relative abundance of miRNA compared with miR-39 as an internal control.

Statistical analysis

Data are expressed as mean ± standard error of the mean (SEM) or median [interquartile range (IQR)] as appropriate. Categorical data are expressed as frequencies and proportions.

The Shapiro–ilk test was used to test for normality of the numerical variables. If normally distributed, the t-test was used to evaluate for differences between two different groups.

If non-normally distributed, non-parametric comparisons for quantitative variables were used to evaluate differences between groups using the Mann–Whitney test. The Spearman correlation test was used to evaluate correlations between two variables.

Linear regression models were used to examine the factors that may affect the values of peripheral PP, central PP and PWV in patients from the clinical study. Variables that were statistically significant in the univariate analysis and others considered clinically relevant were included in the multivariate analysis. Age, which is tightly correlated with PP and PWV, was included in the multivariate analysis as a continuous variable and as a binary variable (older and younger than 60 years) since, as previously established, patients >60 years of age have a higher risk of presenting high values of PP and PWV [27]. We also tested for the interaction between the C-FGF23 and mean blood pressure (MBP) in regression models given that MBP may influence PWV.

SPSS Statistics 15.0 (SPSS, Chicago, IL, USA) and GraphPad Prism 6.0c (GraphPad Software, La Jolla, CA, USA) were used to perform all the statistical analyses. Two-sided *P*-values <.05 were considered statistically significant.

RESULTS

Evidence of a direct effect of FGF23 on inducing a synthetic phenotype in VSMCs

As has been previously described [28, 29], an increase in VSMC proliferation may indicate a change from a contractile to a synthetic phenotype. In cultured VSMCs, the addition of FGF23 (2 and 20 ng/ml) to the medium for a 24-hour period stimulated cell proliferation (Figure 1A) and significantly increased the expression of synthetic markers of VSMCs. This increase in cellular proliferation was further documented by an increase in the expression of cyclin D1 and PCNA (Figure 1B and C).

In cultured VSMCs, the addition of FGF23 decreased the expression of vascular SMA (α-SMA), compatible with a change to a synthetic phenotype, and produces a recognizable change in cell morphology as shown by confocal microscopy (Figure 1D). Control VSMCs cultured without FGF23 exhibited the normal fusiform shape, whereas FGF23-treated VSMCs were not elongated and displayed a rhomboidal morphology (Figure 1D). The cell length:width ratio was significantly decreased in cells incubated with FGF23 (at 2 ng/ml) as compared with controls (5.0 ± 0.3 versus 3.1 ± 0.2, $P < .001$). Moreover, a reduction of α-SMA immunofluorescence was evident after the addition of FGF23 to the medium (Figure 1E). Finally, FGF23 administration increased the amount of MMP9, an extracellular matrix proteinase specific from synthetic phenotype of VSMCs (Figure 1F).

Evidence of a direct effect of FGF23 on the loss of the contractile phenotype of VSMCs

In addition to α-SMA (Figure 1D), FGF23 significantly decreased the gene expression of other specific proteins of the contractile phenotype, such as elastin and MHC (Figure 1G-I). No significant differences were observed between the effects of 2 and 20 ng/ml of FGF23, hence subsequent experiments were performed using 2 ng/ml of FGF23.

FGF23 downregulates the biogenesis of miRNA that may affect normal VSMC function

To identify the mechanisms whereby high levels of FGF23 promote phenotypic switching of VSMCs, an miRNA PCR array specific for cardiovascular disease (from Qiagen) was performed on VSMCs cultured with and without FGF23. This array included the analysis of 84 miRNA related with cardiovascular diseases. Results showed that FGF23 promotes changes in the expression of specific miRNAs associated with cardiovascular diseases. Comparison of miRNA expression in control and FGF23-treated cells showed that FGF23 produces a >1.75-fold decrease in 63 of the 84 miRNAs analysed and in 21 miRNAs the change did not achieve the 1.75-fold change (Table 2). Downregulation of some of these miRNAs, such as miR-23b-3p, miR-24-3p, miR-26a-3p, miR-125a, miR-130a-3p, miR-133b, miR-145-5p, miR-181a, 181b, *miR-221* and miR-, have been previously associated with arterial stiffening and VSMC phenotypic switching [30], suggesting that high levels of FGF23 have a significant effect on the phenotype of VSMCs. The downregulation of some of these miRNAs, such as *miR-221*, *miR-222*, miR-26a and miR-145, was validated by qPCR in four different VSMC cultures (Figure 2A–D).

The FGF23-induced downregulation of a wide number of VSMC miRNAs would suggest that FGF23 could affect some elements involved in VSMC miRNA biogenesis. To test this hypothesis, mRNA expression of key elements for miRNA biogenesis, such as *Drosha*, *Exportin 5*, *AGO1* and *AGO2*, was analysed in VSMCs cultured with high levels of FGF23. Results showed that the expression of these genes was significantly downregulated by high levels of FGF23, explaining the large number of downregulated miRNAs (Figure 2E–H).

Among the analysed miRNAs, *miR-221/222* are particularly relevant since the miRNA 221/222 gene cluster is increased via angiotensin II, while it is downregulated by a repressive complex generated by oestrogen receptor α [31, 32], suggesting an important role in vascular biology and function. Previous studies have suggested that *miR-221/222* are involved in the change of VSMC phenotype, having an impact on vascular function [19, 20], thus we considered that it was important to analyse in more detail the relationship between high levels of FGF23 and *miR-221/222* in VSMCs.

FGF23 modifies VSMC phenotype through FGFR1 phosphorylation

In VSMCs in culture, the addition of FGF23 produces phosphorylation of FGFR1 and Erk1/2. This effect was prevented by AZD4547, an FGFR1 inhibitor (Figure 3A, B) and by PD98059, which inhibits Erk1/2 phosphorylation (Figure 3C, D). AZD4547 also reduced Erk1/2 phosphorylation. These results suggest that the effects of FGF23 on VSMCs are mediated by FGFR1 phosphorylation (Figure 3A, B).

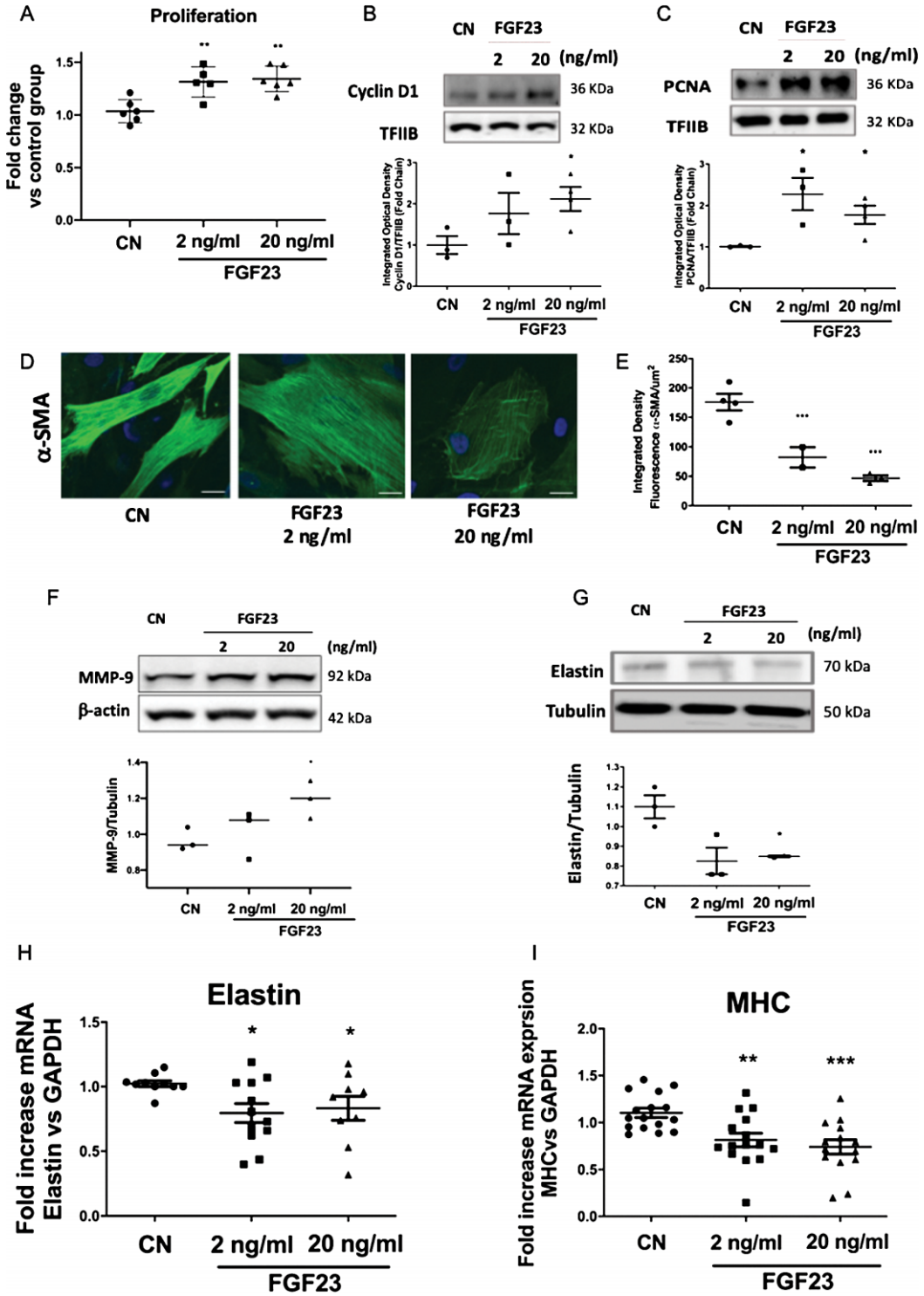

FIGURE 1: FGF23 induces changes in the phenotype of VSMCs. (**A**) After a 24-hour period of culture with human rFGF23 (2 and 20 ng/ml) a significant increase in VSMC proliferation was observed ($n = 6$ in each group, data from three technical replicates [t-test, $^{***}P < .001$ versus controls (CN)]. FGF23 increased the levels of (**B**) cyclin D1 (t-test, $^{*}P < .05$ versus CN) and (**C**) PCNA (t-test, $^{*}P < .05$ versus CN). (**D**) After 9 days in culture, FGF23 reduced α-SMA expression and produced a morphological change in VSMCs from spindle to a less elongated and wider morphology (image representative of three biological replicates). (**E**) Integrated density fluorescence of α-SMA per area was quantified in all VSMCs from three images at 40× from each experiment ($n = 3$, t-test, $^{**}P < .01$ and $^{***}P < .001$ versus CN). (**F**) The amount of MMP9 increased significantly after the addition of FGF23 at 20 ng/ml; western blot and quantification from three different cultures (t-test, $^{*}P < .05$ versus CN). (**G**) The amount of elastin, a contractile protein, decreased after 9 days of culture with human FGF23; western blot and quantification from three different cultures (t-test, $^{*}P < .05$ versus CN). Similarly, after 9 days, FGF23 decreased the mRNA expression of specific contractile genes such as (**G**) elastin (t-test, $^{*}P < .05$ versus CN) or (**H**) MHC (t-test, $^{**}P < .01$ versus CN, $^{***}P < .001$ versus CN). (For RT-PCR analysis, six biological replicates were obtained from three different experiments (12 per group). Data presented as mean ± standard deviation.

Table 2. miRNA PCR array specific for cardiovascular disease in FGF23-treated VSMCs versus controls

miRNA		miRNA		miRNA	
let-7a-5p	–	miR-15b-5p	=	miR-29b-3p	=
let-7b-5p	–	miR-16-5p	–	miR-29c-3p	=
let-7c-5p	–	miR-17-5p	–	miR-302a-3p	–
let-7d-5p	–	miR-181a-5p	–	miR-302b-3p	–
let-7e-5p	–	miR-181b-5p	–	miR-30a-5p	–
let-7f-5p	–	miR-182-5p	=	miR-30c-5p	–
miR-1-3p	–	miR-183-5p	–	miR-30d-5p	–
miR-100-5p	–	miR-185-5p	–	miR-30e-5p	–
miR-103a-3p	=	miR-18b-5p	=	miR-31-5p	–
miR-107	=	miR-195-5p	–	miR-320a	–
miR-10b-5p	–	miR-199a-5p	–	miR-328-3p	–
miR-122-5p	=	miR-206	=	miR-342-3p	–
miR-124-3p	=	miR-208a-3p	–	miR-365b-3p	–
miR-125a-5p	–	miR-208b-3p	–	miR-378a-3p	–
miR-125b-5p	–	miR-22-3p	=	miR-423-3p	–
miR-126-3p	=	miR-221-3p	–	miR-424-5p	–
miR-130a-3p	–	miR-222-3p	–	miR-451a	=
miR-133a-3p	=	miR-223-3p	–	miR-486-5p	–
miR-133b	–	miR-224-5p	–	miR-494-3p	=
miR-140-5p	–	miR-23a-3p	–	miR-499a-5p	=
miR-142-3p	=	miR-23b-3p	–	miR-7-5p	–
miR-143-3p	–	miR-24-3p	–	miR-92a-3p	–
miR-144-3p	–	miR-25-3p	–	miR-93-5p	–
miR-145-5p	–	miR-26a-5p	–	miR-98-5p	–
miR-146a-5p	=	miR-26b-5p	–	miR-99a-5p	=
miR-149-5p	–	miR-27a-3p	=	miR-21-5p	–
miR-150-5p	–	miR-27b-3p	–	miR-210-3p	=
miR-155-5p	–	miR-29a-3p	–	miR-214-3p	–

– : downregulated miRNA expression versus control cells;
= : miRNA without change.

Blockade of FGF23 actions by the inhibition of FGFR1 or ErK1/2 phosphorylation using AZD4547 or PD98059 produced a marked increase in the expression of VSMC contractile genes such as elastin and MHC (Figure 3E, F).

FGF23 modifies the VSMC phenotype by reducing the expression of *miR-221/222*

The expression of miR221/222 was measured in FGF23-treated VSMCs incubated with the FGFR1 or Erk1/2 inhibitors AZD4547 and PD98059, respectively. Inhibition of FGFR1 produced a significant increase in *miR-221* expression ($P = .022$) and no change in *miR-222* ($P = .959$) (Figure 3G, H). PD98059 administration did not modify *miR-221* or *miR-222* expression, suggesting that the phosphorylation of Erk1/2 is not necessary to modify *miR-221/222* expression (Figure 3I, J).

Both miRNA-221 and -222 were transfected into VSMCs to determine to what extent the reduction of these miRNAs was responsible for the FGF23-mediated phenotypic transition of VSMCs. After a 9-day culture with FGF23, VSMCs were transfected with Scrambled (SCR), miRNA-221-3p mimic or miRNA-222-3p mimic for 48 hours, resulting in increased expression of both *miR-221-3p* and *miR-222-3p* (Figure 4A, B).

VSMCs transfected with *miR-221-3p* mimic showed an increased expression of elastin (Figure 4C) and MHC (Figure 4D). However, in VSMCs transfected with *miR-222-3p* mimic, the effects on elastin and MHC did not reach statistical significance (Figure 4E, F).

A reduction in *miR-221/222* increases MAP3K2 and PAK1 expression with a concomitant phosphorylation of ERK1/2, a mechanism whereby FGF23 may induce a VSMC synthetic phenotype

According to databases such as TargetScan and mirDB, the MAP3K2 and PAK1 proteins are targets of *miR-221/222*. In VSMC culture, the addition of FGF23, which downregulates *miR-221/222* expression, produced a significant increase in the gene expression of MAP3K2 and PAK1 (Figure 4G, H). Transfection of *miR-221* or *miR-222* prevented an increase in mRNA expression of MAP3K2 and PAK1 (Figure 4G, H). It should be noted that *miR-221* and *miR-222* transfections caused a decrease in Erk1/2 phosphorylation (Figure 4I), suggesting that MAP3K2, PAK1 and Erk1/2 phosphorylation participate as a mechanism whereby FGF23 promotes a VSMC synthetic phenotype.

The Supplemental material Figure S1 shows the results obtained using anti-mimic transfections of *miR-221* and *miR-222* in VSMCs. After 48 hours, there was a significant reduction of *miR-221* expression that was almost significant for *miR-222* ($P = .0537$). A significant statistical correlation was found between the expression of both miRNAs and elastin (Figure S1C, D). These results suggest an association between the values of these miRNAs and the expression of this contractile marker of VSMCs.

Recombinant klotho administration did not modify the synthetic phenotype of VSMCs induced by FGF23

The administration of recombinant klotho at 20 ng/ml for 9 days in the presence of rFGF23 (2 ng/ml) did not modify the expression of elastin and MHC, suggesting that the pro-synthetic effects of FGF23 on VSMCs are independent of klotho (Supplementary material, Figure S2).

Continuous infusion of exogenous FGF23 promotes phenotypic switching of VSMCs from rat aortas

Rats receiving a continuous infusion of rFGF23 through a subcutaneously implanted Alzet pump showed the expected increase in FGF23 levels (from 301 ± 117 to 811 ± 224 pg/ml; $P < .001$), which was accompanied by phosphaturia and a moderate reduction in the concentration of serum phosphate (6.3 ± 0.9 versus 5.7 ± 0.9 mg/dl). In rats receiving rFGF23, the amount of *miR-221-3p* measured in the abdominal aorta was significantly decreased as compared with the vehicle group, however, there was not change in aortic levels of *miR-222-3p* (Figure 5A, B). FGF23 infusion caused a reduction in the mRNA expression of elastin and MHC (Figure 5C, D). The amount of elastin in the thoracic aorta was analysed by immunohistochemistry. VSMCs from the aorta of rats that received FGF23 for 14 days had lower amounts of elastin than rats from the vehicle group (Figure 5E–H).

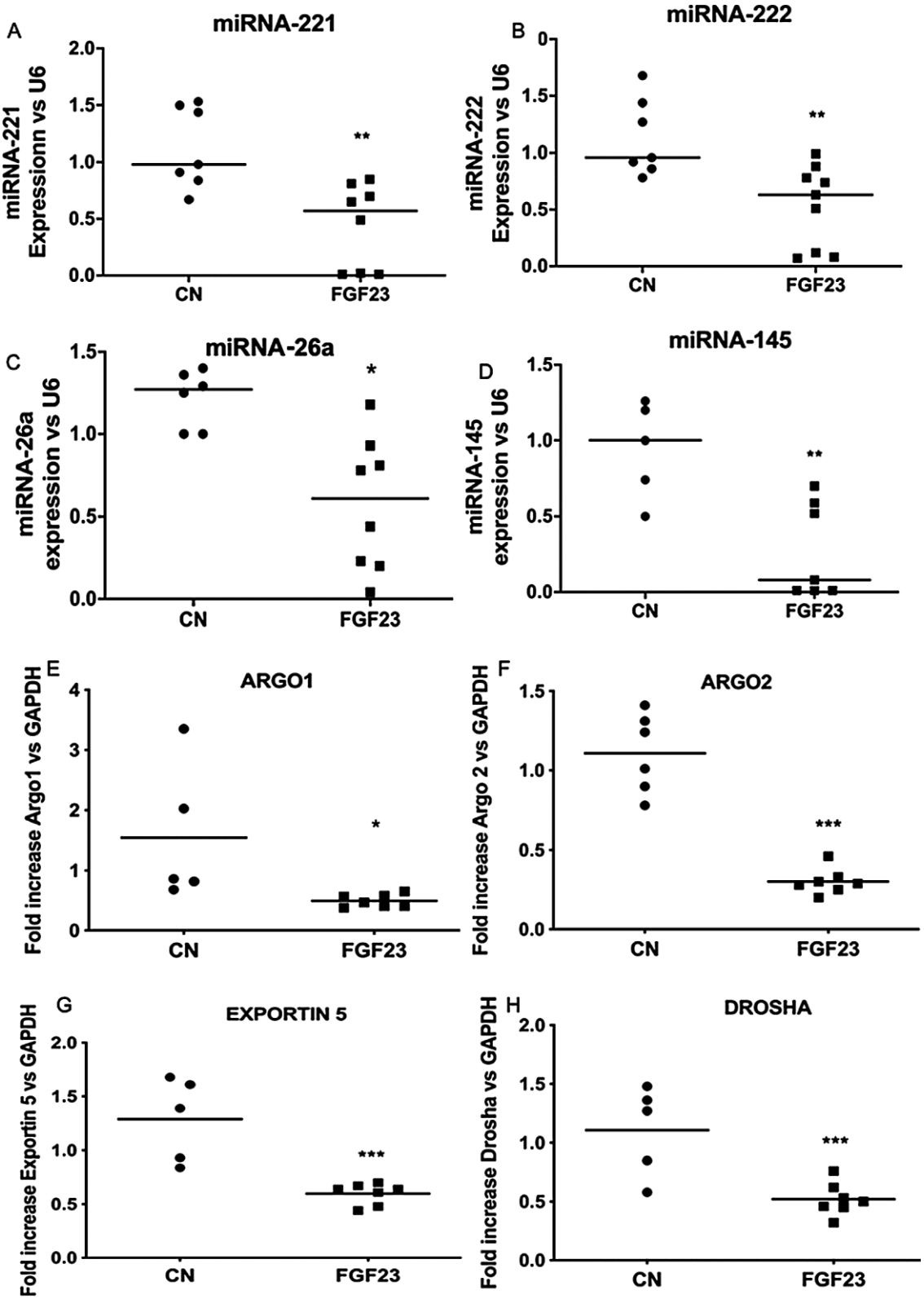

FIGURE 2: Effects of rFGF23 on miRNA expression related to arterial stiffening and miRNA biogenesis. In VSMCs, a 9-day culture with rFGF23 produced a downregulation of a large number of miRNAs related to cardiovascular dysfunction. In relation to VSMC phenotypic switching and arterial stiffening, there was a decrease in the expression of miRNAs, including (**A**) *miR-221-3p*, (**B**) *miR-222-3p*, (**C**) miR-26a and (**D**) miR-145-5p [*t*-test, $^{*}P < .05$, $^{**}P < .01$ versus controls (CN)]. The large number of miRNAs showing a decreased expression might be the consequence of a downregulation of several elements involved in miRNA biogenesis, including (**E**) argonaute 1, (**F**) argonaute 2, (**G**) *exportin 5* and (**H**) Drosha (*t*-test, $^{*}P < .05$ and $^{***}P < .001$ versus CN) ($n = 6$ versus 7 from three different cultures). Data presented as mean ± standard deviation.

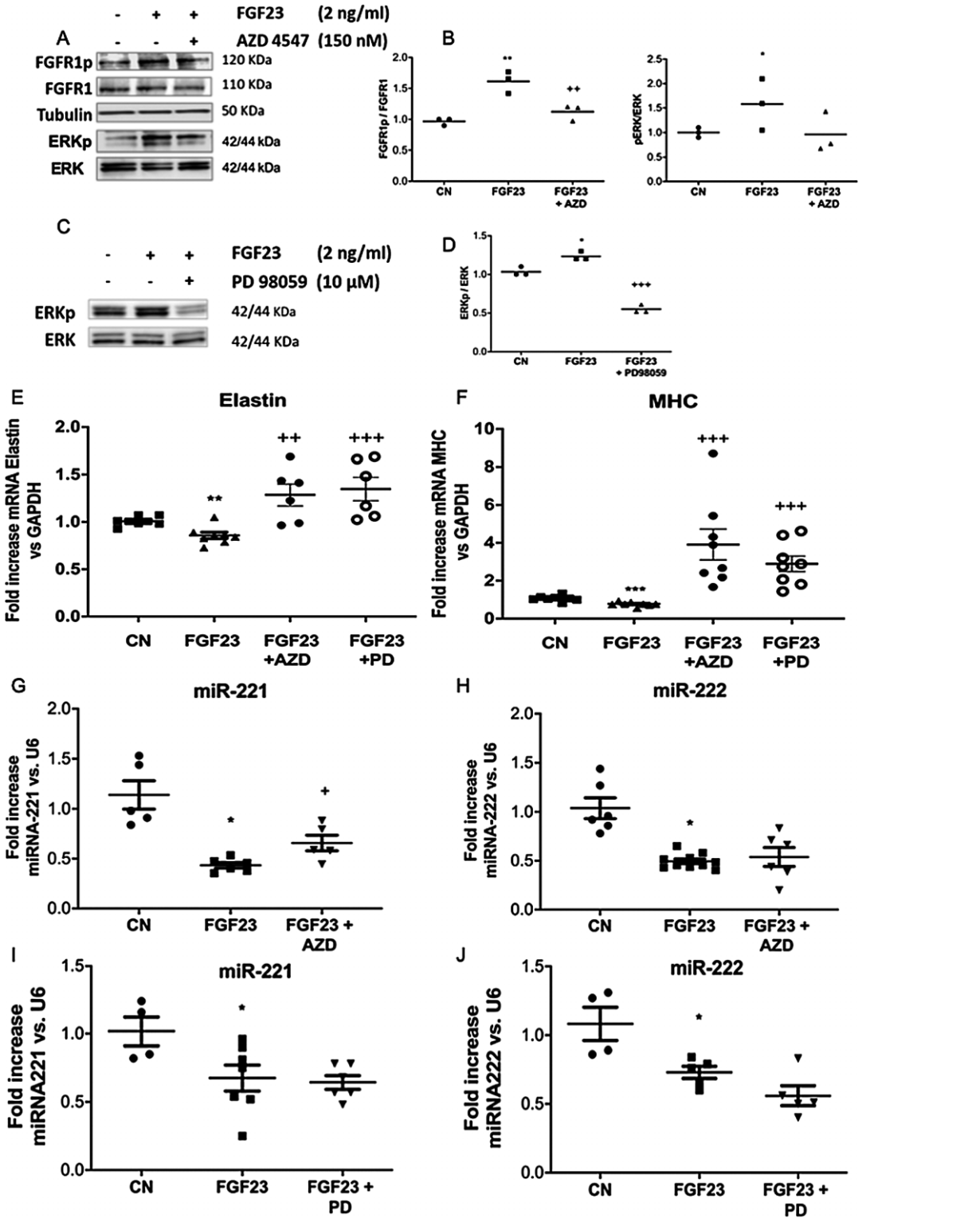

FIGURE 3: The effects of FGF23 on VSMCs are mediated by FGFR1 and Erk1/2 activation. (**A**) A 6-h treatment with FGF23 produced an increase in FGFR1 phosphorylation [$^{**}P < .01$ versus controls (CN)] while inhibition of FGFR1 by AZD4547 decreased this phosphorylation (t-test $^{++}P < .01$ versus FGF23). FGF23 increased Erk1/2 phosphorylation and AZD4547 reduced it (t-test, $^{*}P < .05$ versus CN). Unphosphorylated Erk1/2 was used as a housekeeper band. (**B**) Quantification of western blots. The phosphorylation of Erk1/2 decreased by the administration of PD98059 (10 μM) and its quantification is shown in (**C**) and (**D**) (t-test $^{+++}P < 001$ versus FGF23). The addition of both FGFR1 and Erk1/2 inhibitors to cells cultured with FGF23 for 9 days increased the expression of VSMC contractile markers such as (**E**) elastin (Mann–Whitney test, $^{**}P < .01$ versus CN, 1.00 ± 0.05 versus 0.85 ± 0.09 and $^{++}P < .01$, $^{+++}P < .001$ versus FGF23 group) and (**F**) MHC ($^{***}P < .001$ versus CN, 1.06 ± 0.14 versus 0.76 ± 0.11 and $^{+++}P < .001$ versus FGF23 group). (**G**) FGFR1 inhibition by AZD4547 (150 nM) significantly increased *miR-221* expression (t-test, $^{*}P < .05$) but not (**H**) *miR-222*. In the presence of FGF23, Erk1/2 inhibition by PD98059 did not modify (**I**) *miR-221* and (**J**) *miR-222* expression. ($n = 9$ per group, three technical replicates). Data presented as mean $\pm$ standard deviation.

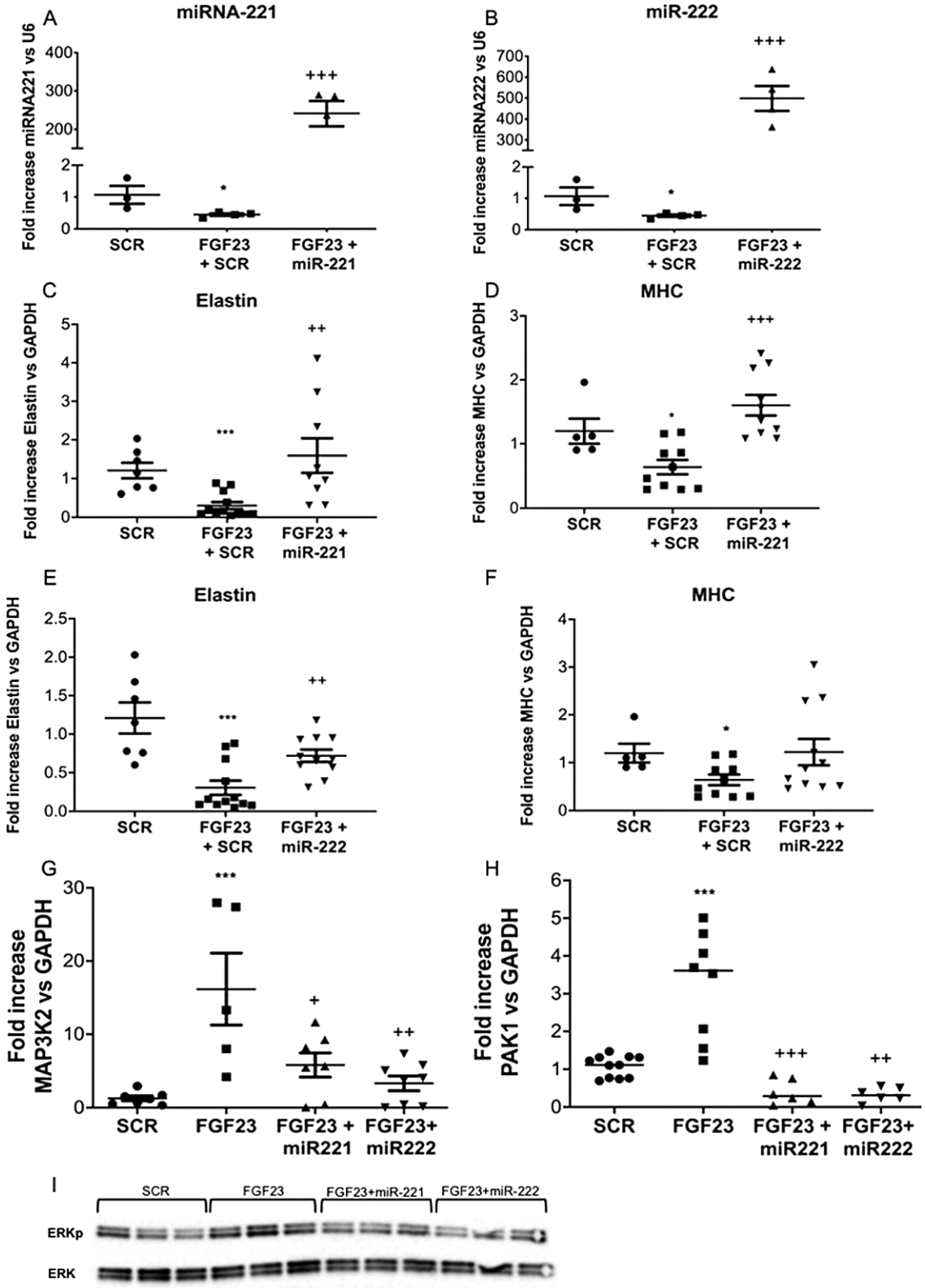

FIGURE 4: Phenotypic transition of VSMCs induced by high FGF23 is mediated by a decrease in *miR-221* and *miR-222*. The transfection of (**A**) *miR-221* and (**B**) *miR-222* increased the respective expression of each miRNA despite the presence of high levels of FGF23. The transfection of *miR-221* increased the expression of (**C**) elastin (*t*-test, $^{++}P < .01$ versus FGF23 + SCR) and (**D**) MHC (*t*-test, $^{+++}P < .001$ versus FGF23 + SCR). The transfection of *miR-222* to VSMCs increased significantly the expression of (**E**) elastin (*t*-test, $^{++}P < .01$ versus FGF23 + SCR) but not (**F**) MHC. VSMCs cultured with FGF23 for 9 days increased the expression of (**G**) MAP3K2 [*t*-test, $^{***}P < .001$ versus controls (CN)] and (**H**) PAK1 (*t*-test, $^{**}P < .01$ versus CN). The transfection of *miR-221* and *miR-222* decreased the expression of MAP3K2 and (**H**) PAK1 despite the presence of FGF23 (*t*-test, $^{+++}P < .001$, $^{++}P < .01$ and $^{+}P < .05$ versus FGF23). (**I**) FGF23-induced Erk1/2 phosphorylation was reduced by *miR-221* and *miR-222* transfection. ($n = 9$ per group, three technical replicates). Data presented as mean ± standard deviation.

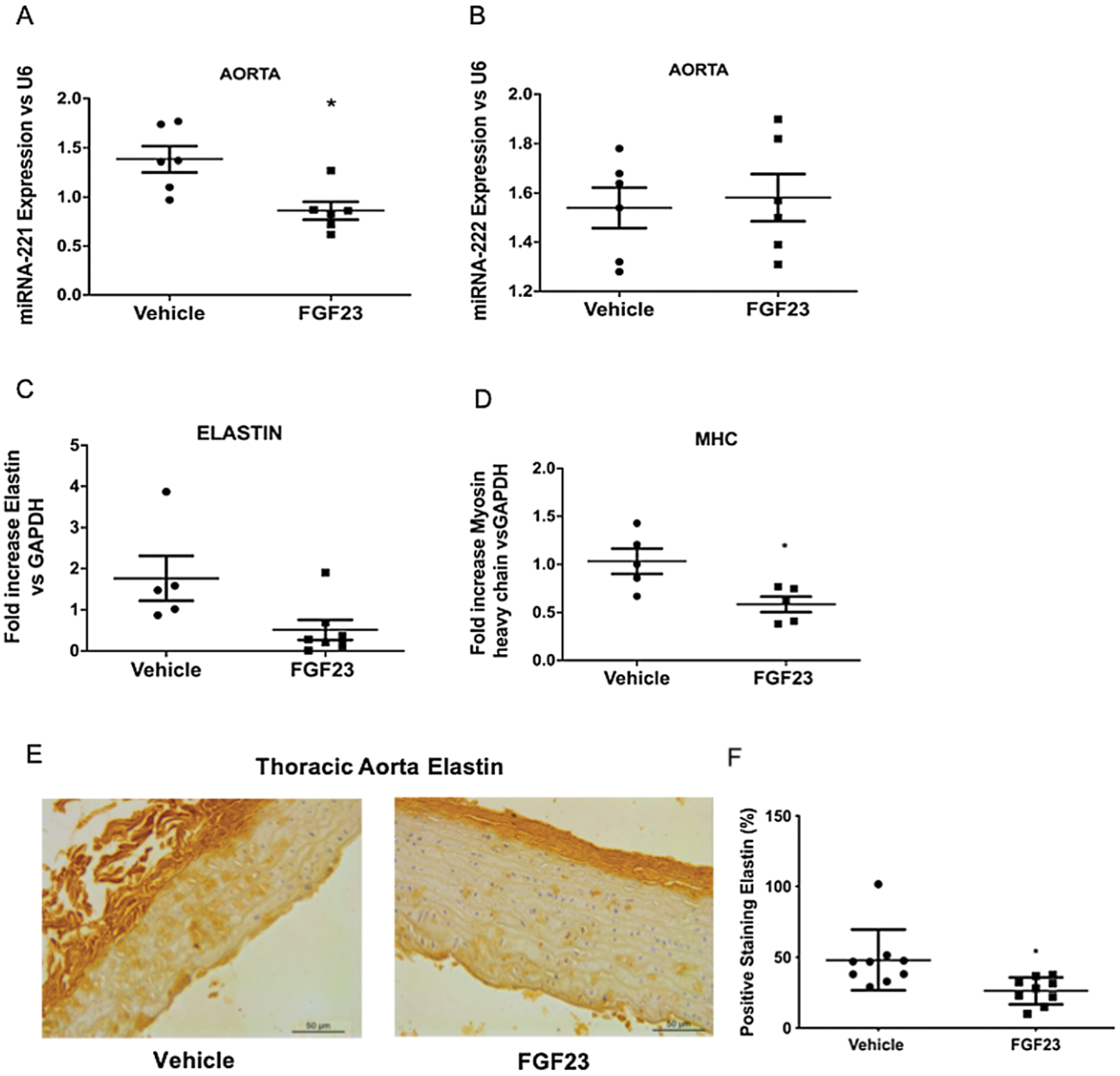

FIGURE 5: The *in vivo* infusion of rFGF23 produced changes in aortic *miR-221* and in contractile markers of VSMCs. A 14-day infusion of rat rFGF23 produced a significant decrease of (**A**) *miR-221* levels in the aorta; however, there was not a significant change in the level of (**B**) *miR-222*. ($n = 6$ animals per group, *t*-test, $^*P < .05$ versus vehicle). In the aorta, the mRNA expression of (**C**) elastin and (**D**) MHC was reduced after FGF23 administration ($n = 5$ for each group, *t*-test, $^*P < .05$ versus vehicle). (**E**) Elastin immunohistochemistry was performed in thoracic aortas from vehicle and FGF23-treated rats with lesser staining in animals with infusion of rFGF23 (image at 10×, scale bar 50 μm representative from six different immunohistochemistry tests). (**F**) Positive staining for elastin was quantified with ImageJ software as a percentage of positive staining per area in both groups.

Histological analysis of rat aortas receiving FGF23 infusion

Haematoxylin and eosin staining of thoracic aortas revealed that the thickness of the median layer was increased in rats receiving FGF23 as compared with rats receiving vehicle ($P < .05$ versus vehicle group; Table 3). In addition, there was a marked change in the orientation of the nuclei of the VSMCs. As shown in Figure 6A and Table 3, the aortas from vehicle rats had VSMCs with elongated cell nuclei that were oriented parallel to the elastic fibres. In contrast, in FGF23-treated rats, most VSMC nuclei were positioned almost perpendicular to the elastic fibres. Similarly, picrosirius red staining revealed that FGF23 administration increased the deposition of extracellular matrix, another marker of the synthetic phenotype of VSMCs (Figure 6B). Confocal microscopy was also used to visualize picrosirius red staining of thoracic aortas, showing greater extracellular matrix deposition in FGF23 treated rats than vehicle rats (Figure 6C). In thoracic aortas from

Table 3. Thoracic aortic structure and haemodynamic parameters

Characteristics	Vehicle	FGF23	*P*-value
Media thickness (μm)	186.8 ± 15.56	266.4 ± 26.56	<.05
Nuclear cell orientation (°)	24.7 ± 2.08	69.9 ± 1.66	<.001
PP (mmHg)	19.4 ± 1.29	26.2 ± 2.48	<.05
Systolic BP (mmHg)	125.4 ± 3.51	127.2 ± 2206	ns
Diastolic pressure (mmHg)	106 ± 3.37	101.1 ± 4.2	ns
BPM	433.8 ± 5.09	445.3 ± 7.56	ns

Aorta media thickness was measured using ImageJ software from haematoxylin and eosin (H&E) images of vehicle and FGF23-treated rats ($n = 6$ per group). Images were obtained at 20× (scale bar 50 μm) and six measurements from each thoracic aorta were performed. The average width of the tunica media was obtained as the mean of four measurements taken at 0°, 90°, 180° and 270° around the sectional circumference of the aorta stained by H&E. (*t*-test, $P < .05$ versus vehicle).

The angles formed by the nuclei with respect to the elastic fibre was also measured in four different microphotographs from each aorta and animal. All nuclei from each image were measured. ImageJ software was also used to obtain these measurements (*t*-test, $P < .001$ versus vehicle). At 14 days, PP was higher in FGF23-treated animals than in vehicle rats (*t*-test, $P < .05$ versus vehicle). Systolic and diastolic BP and beats per minute were similar in both groups. Results are presented as mean ± standard error of the mean.

ns: not significant.

rFGF23-treated rats there was also an increased presence of the synthetic markers of VSMCs, fibronectin and MMP9 (Figure 6D, E). Histological quantification of picrosirius red, fibronectin and MMP9 showed significant differences between vehicle and FGF23-treated rats (Supplementary material, Figure S3).

Finally, as compared with controls, rats receiving FGF23 had a slight increase in systolic BP and a mild decrease in diastolic BP that were not significant. However, the PP was significantly greater in rats receiving the infusion of FGF23, suggesting an increase of arterial stiffness. Heart frequency in beats per minute (bpm) were not different in vehicle and FGF23 rats (Table 3).

Passive and active force of aorta arterial rings from rats treated with FGF23

In the context of uraemia, the *in vivo* effects of high levels of FGF23 on endothelial cells have already been described in different works [7, 8]. However, a specific effect of FGF23 on VSMC contractibility has not yet been explored. To analyse whether the structural changes previously described had functional consequences, the elasticity and stiffness of aortic rings were tested in a wire myograph. Initially we tested if a short exposure (2 h) of rFGF23 at 2, 20 and 100 ng/ml produced changes in elasticity and stiffness in aortic rings from control rats. In these conditions, there were not significant changes observed with respect to aortic rings without FGF23 (data not shown). The next experiment was designed to test changes in the elasticity and stiffness of aortic rings from animals that had received FGF23 infusion for 14 days as compared with the vehicle group. Thus arterial rings were mechanically stretched using a micropositioner. Simultaneously, changes in wall tension (passive force) were measured with a sensitive force transducer until transmural pressure reached 100 mmHg (vessel normalization). Figure 7A, B show representative tracings of the force generated in arterial rings from animals treated with vehicle or FGF23. Under similar stretch conditions, the force evoked by arterial rings was greater in animals treated with FGF23 than in controls. Moreover, arterial rings from FGF23-infused rats required a significantly smaller stretch to reach 100 mmHg of transmural pressure than arterial rings from rats treated with vehicle (∼1387 ± 83.57 μm vehicle versus ∼1049 ± 89.04 μm FGF23) (Figure 7C). To ensure that the alterations observed in passive properties were due to changes in arterial wall structure, a stress–strain analysis was performed. Wall stress was increased in rings from animals treated with FGF23. This difference was significant when stretch reached a value of 0.45 (Figure 6D). After normalization, arterial rings from rats that had received FGF23 or vehicle were stabilized for 1 hour and then treated with vasoactive stimuli: high potassium solution (70K; Figure 6E) and noradrenaline (Figure 6F); a different vasoconstrictor effect was observed in the vehicle and FGF23-treated rats. Arterial rings from rats treated with FGF23 showed a significant reduction in vasoconstrictor response to 70K (∼19.02 mN in vehicle and ∼15.62 mN in FGF23) and to noradrenaline (∼23.45 mN in vehicle and ∼16.74 mN in FGF23) (Figure 6G, H, respectively).

Relationship between plasma concentration of C-FGF23, parameters of arterial stiffness and plasma levels of *miR-221* and *miR-222* in patients with CKD stage 2–3

The clinical characteristics and biochemical parameters of 76 CKD stage 2–3 and metabolic syndrome patients are shown in Table 4. Serum phosphate concentration was within the normal range. As expected, serum C-FGF23 levels were increased and showed a significant inverse correlation with the estimated glomerular filtration rate (eGFR) (Table 5). A significant correlation was also observed between C-FGF23 levels and parameters of arterial stiffening such as peripheral and central PP ($P = .006$ and $P = .013$, respectively) and PWV ($P = .013$).

A multivariable linear regression analysis revealed that peripherical PP, central PP and PWV correlated with C-FGF23 independent of the eGFR and age (Tables 6–8). In a multivariate regression analysis with PWV as the dependent variable (Table 8), C-FGF23 showed an interaction with MBP in predicting PWV, suggesting that the effect of C-FGF23 on PWV is broader as MBP increases.

The plasma levels of *miR-221-3p* and *miR-222-3p* were measured in patients with the highest and lowest values of C-FGF23 (highest and lowest deciles). The values of *miR-221-3p* and *miR-222-3p* were lower in patients with high C-FGF23 as compared with low C-FGF23 (Figure 8A, B).

DISCUSSION

The results of the present study show that FGF23 stimulates phenotype switching of VSMCs from a contractile to a synthetic phenotype, which increases wall thickness and arterial stiffening in rats. In patients with CKD stage 2–3, these changes are associated with an increase in PWV. Our finding from experiments *in vitro*, *in vivo* and *ex vivo* and data from patients supports the concept of a direct action of FGF23 on VSMCs.

In cultured VSMCs, high levels of FGF23 decrease miRNA biogenesis, thus reducing the expression of miRNAs involved in vascular dysfunction, such as miR-26a, miR-145, *miR-221*

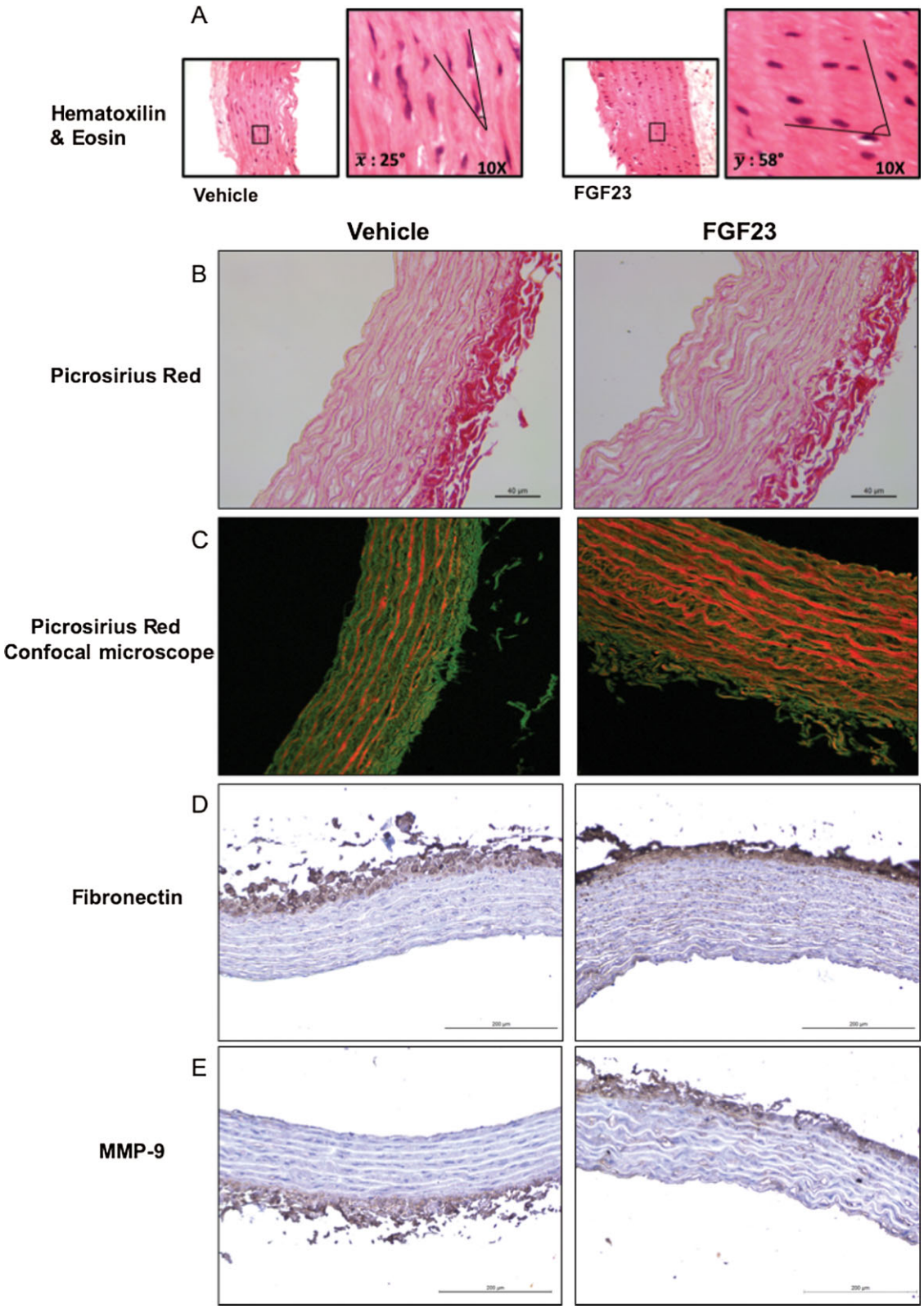

FIGURE 6: The *in vivo* infusion of recombinant FGF23 produced changes in synthetic markers of VSMCs. (A) Haematoxylin and eosin staining of rat thoracic aorta revealed morphologic changes in tunica media cells. Representative images at 10× from each group of rats are shown. (**B**) Picrosirius staining of aortas from the vehicle and rFGF23 groups. In rats with rFGF23 infusion, the elastic fibres are disorganized with a tunica media that is wide with abundant deposition of extracellular matrix (a representative image at 40 μm of each group is shown). (**C**) Picrosirius visualization using confocal microscopy exciting at 633–754 nm revealed, with more detail than optical images, the changes in fibre elastic organization and the extracellular matrix deposition around these fibres in FGF23 as compared with the vehicle-treated group. (Representative image at 10× for each group). The presence of (**D**) fibronectin and (**E**) MMP9 was higher in FGF23 than vehicle-treated rats. (Scale bar 200 μm, representative image for each group).

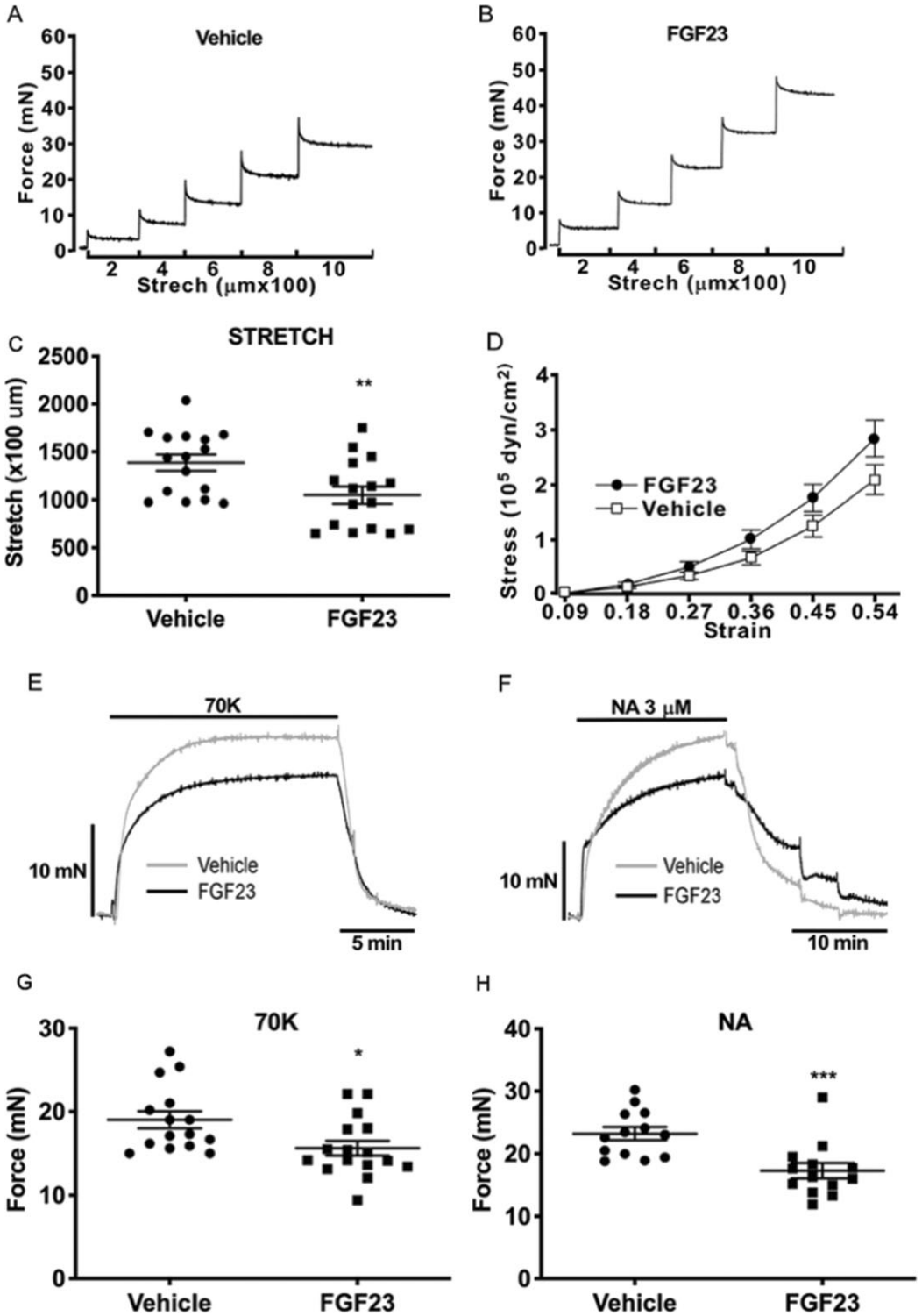

FIGURE 7: High FGF23 induced changes in passive and active arterial wall tension. Representative recordings during the normalization process in aortic rings from rats treated with (**A**) vehicle or (**B**) FGF23. (**C**) Arterial rings from rats treated with FGF23 required less stretch to reach a transmural pressure of 100 mm Hg (FGF23: stretch ∼1049 μm; vehicle: stretch ∼1387 μm). Number of animals: vehicle, 4 (16 rings); FGF23, 4 (16 rings). $^{**}P < .01$ versus vehicle. (**D**) Strain–stress relationship in arterial rings treated with vehicle or FGF23. The Mann–Whitney test was used to evaluate differences between groups when a normal distribution was not observed (strain = 0, 0.09, 0.18, 0.27, 0.36). Student's *t*-test was used to evaluate differences between groups when a normal distribution was observed (strain = 0.45). Strain is calculated as the increase in internal circumference divided by the initial internal circumference. Then the units of length are cancelled and it remains as a dimensionless variable. Number of animals: vehicle, 4 (16 rings); FGF23, 4 (16 rings). $^{*}P < .05$ versus vehicle. Representative records of arterial contraction induced by (**E**) 70K or (**F**) noradrenaline in aortic rings of vehicle or FGF23-treated rats. Quantitative analysis of isometric force generated in arterial rings in response to either (**G**) 70K or (**H**) noradrenaline. (The Mann–Whitney test was used to evaluate differences between groups. $^{**}P < .01$, $^{***}P < .001$ versus vehicle. Number of animals for 70K: vehicle, 4 (15 rings); FGF23, 4 (16 rings). Number of animals for noradrenaline: vehicle, 3 (10 rings); FGF23, 3 (11 rings). Data are presented as mean ± standard error.

Table 4. Main characteristics and biochemical parameters for serum and urine of patients included in the study ($N = 76$)

Parameter	Values
Age (years)	61.2 (9.4)
Sex (female/male), *n*/*n*)	20/56
BMI (kg/m^2)	32.6 (4.3)
Abdominal perimeter (cm)	111 (11)
Systolic BP (mmHg)	138 (19)
Diastolic BP (mmHg)	85 (12)
Peripheral PP (mmHg)	53 (13)
Heart rate (bpm)	64 (10)
Smokers/ex-smokers, *n*/*n*	8/24
Antidiabetic treatment, *n*	37
Dyslipidaemia treatment, *n*	59
Antihypertensive treatment, *n*	72
ACEI, *n*	8
ARB, *n*	63
Diuretics, *n*	43
CCB (D), *n*	47
BB, *n*	27
CAB, *n*	32
Other antihypertensive drugs, *n*)	4
eGFR (CKD-EPI; ml/min/1.73 m^2)	67 (21)
Serum creatinine (mg/dl)	1.19 (0.4)
Serum phosphate (mg/dl)	3.1 (0.5)
FeP (%)	24.1 (10.3)
FeP 24-hour (%)	21.9 (9.1)
Phosphate:creatinine ratio (mg/mg)	0.59 (0.15)
Phosphate:creatinine ratio 24-hour (mg/mg)	0.59 (0.16)
C-FGF23 (RU/mL)	86.7 (35)
Central systolic BP (mmHg)	127 (17)
Central diastolic BP (mmHg)	87 (12)
Central PP (mmHg)	40 (11)
PWV (m/s)	9.1 (1.5)
Cardiac output (l/min)	3.9 (0.7)
Cardiac index (l/min/m^2)	1.9 (0.4)
Peripheral vascular resistance (mmHg/ml)	1.5 (0.2)

Values presented as mean (SD) unless stated otherwise.
SD: standard deviation; BMI: body mass index; ACEi: angiotensin-converting enzyme inhibitor; ARB: angiotensin receptor blocker; CCB (D): calcium channels blocker (dihydropyridine); BB: beta-blocker; CAB: central alpha-blocker; eGFR: estimated glomerular filtration rate; CKD-EPI: Chronic Kidney Disease Epidemiology Collaboration; FeP: fractional excretion of phosphate from the first morning void and from a 24-h urine collection.

Table 5. Correlation of C-FGF23 with independent variables

Characteristics	Spearman coefficient	*P*-value
Age (years)	0.25	.032
Serum creatinine (mg/dl)	0.48	.0001
eGFR (CKD-EPI; ml/min/1.73 m^2)	−0.61	.0001
Serum phosphate (mg/dL)	0.17	.152
FeP 24-hour (%)	0.45	.002
Systolic BP (mmHg)	0.15	.213
Diastolic BP (mmHg)	−0.12	.300
Peripheral PP (mmHg)	0.33	.006
MBP (mmHg)	0.01	.902
Central systolic BP (mmHg)	0.13	.279
Central diastolic BP (mmHg)	−0.12	.311
Central PP (mmHg)	0.30	.013
PWV (m/s)	0.30	.013
Cardiac output (l/min)	0.01	.878
Cardiac index (l/min/m^2)	0.01	.885
Peripheral vascular resistance (mmHg/ml)	−0.02	.819

eGFR: estimated glomerular filtration rate; CKD-EPI: Chronic Kidney Disease Epidemiology Collaboration; FeP 24-hour: fractional excretion of phosphate from a 24-hour urine collection.

Table 6. Multivariable linear regression: dependent variable peripheral PP

Variables	Beta*	95% CI	*P*-value
Model 1			
Age (years)	0.29	0.055–0.736	.024
eGFR (CKD-EPI; ml/min/1.73 m^2)	0.10	−0.117–0.246	.481
C-FGF23 (RU/mL)	0.34	0.02–0.232	.021
Model 2			
Age (years)			
<60	Ref	0.54–13.4	.034
>60	0.26		
eGFR (CKD-EPI; ml/min/1.73 m^2)	0.11	−0.115–0.258	.446
C-FGF23 (RU/mL)	0.41	0.04–0.26	.007

CI: confidence interval; eGFR: estimated glomerular filtration rate; CKD-EPI: Chronic Kidney Disease Epidemiology Collaboration.
*Standardized regression coefficient.
Model 1: adjusted for age, eGFR (CKD-EPI) and C-FGF23.
Model 2: adjusted for age as a binary variable, eGFR (CKD-EPI) and C-FGF23.

Table 7. Multivariable linear regression: dependent variable central PP

Variables	Beta*	95% CI	*P*-value
Model 1			
Age (years)	0.102	−0.184–0.428	.428
eGFR (CKD-EPI; ml/min/1.73 m^2)	0.017	−0.154–0.172	.911
C-FGF23 (RU/mL)	0.363	0.023–0.213	.016
Model 2			
Age (years)			
<60	Ref	−2.55–8.91	.271
>60	0.14		
eGFR (CKD-EPI; ml/min/1.73 m^2)	0.04	−0.14–0.18	.787
C-FGF23 (RU/mL)	0.40	0.03–0.22	.011

CI: confidence interval; eGFR: estimated glomerular filtration rate; CKD-EPI: Chronic Kidney Disease Epidemiology Collaboration.
*Standardized regression coefficient.
Model 1: adjusted for age, eGFR (CKD-EPI) and C-FGF23.
Model 2: adjusted for age as a binary variable, eGFR (CKD-EPI) and C-FGF23.

Table 8. Multivariable linear regression: dependent variable PWV

Variables	Beta*	95% CI	*P*-value
Model 1			
Age (years)	0.890	0.133–0.151	<.001
eGFR (CKD-EPI; ml/min/1.73 m^2)	0.011	−0.004–0.005	.729
MBP (mmHg)	0.369	0.035—0.046	<.001
C-FGF23 (RU/mL)	0.073	0.000–0.006	.027
C-FGF23*MBP interaction	0.066	0.000–0.000	.015
Model 2			
Age (years)			<0.001
<60	Ref	2.054–2.742	
>60	0.784		
eGFR (CKD-EPI; ml/min/1.73 m^2)	0.024	−0.008–0.012	.726
MBP (mmHg)	0.323	0.024—0.047	<.001
C-FGF23 (RU/mL)	0.311	0.008–0.020	<.001
C-FGF23*MBP interaction	0.150	0.000–0.001	.009

CI: confidence interval; eGFR: estimated glomerular filtration rate; CKD-EPI: Chronic Kidney Disease Epidemiology Collaboration.
*Standardized regression coefficient.
Model 1: adjusted for age, eGFR (CKD-EPI) and C-FGF23.
Model 2: adjusted for age as a binary variable, eGFR (CKD-EPI) and C-FGF23.

and *miR-222*. The addition of FGF23 to human VSMCs not only reduces *miR-221* and *miR-222* levels, but also produces an increase in MAP3K2 and PAK1 expression, which are target genes of *miR-221* and *miR-222*.

Furthermore, the effects of FGF23 on the VSMC phenotype are mediated by FGFR1 and Erk1/2 phosphorylation. The

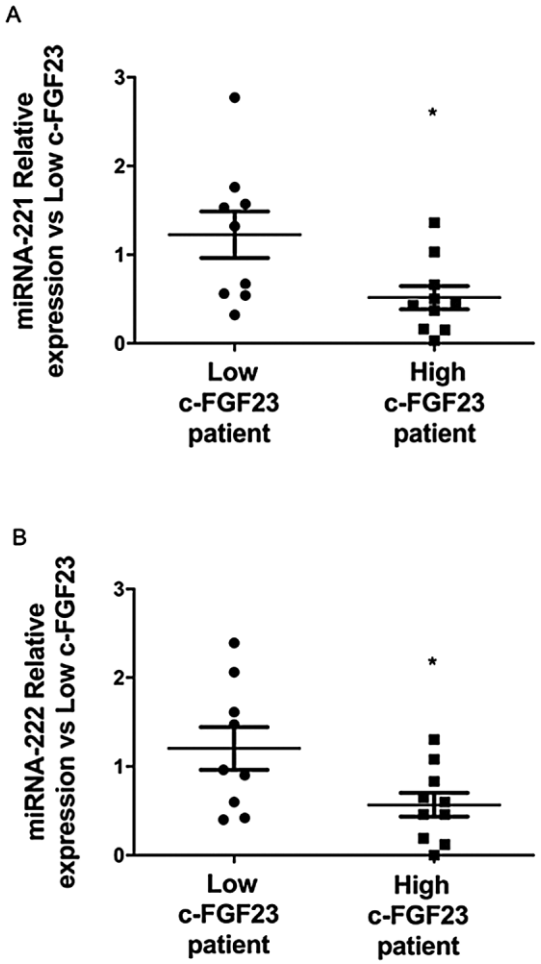

FIGURE 8: Plasma levels of *miR-221* and *miR-222* in CKD stage 2–3 patients with metabolic syndrome are influenced by high levels of FGF23. Plasma levels of FGF23 were measured in 76 patients with CKD stage 2–3 and metabolic syndrome. Plasma levels of (**A**) *miR-221* and (**B**) *miR-222* were measured in those patients with the highest and lowest FGF23 values, corresponding to decile 1 (7 patients, range 148–171 pg/ml) and decile 10 (7 patients, range 34–52 pg/ml) of FGF23. Patients with the highest concentrations of FGF23 had lower plasma levels of *miR-221* and *miR-222* than patients with the lowest FGF23 values (*t*-test, $^*P < .05$ versus low C-FGF23 patients). Data presented as mean ± standard deviation.

inhibition of FGFR1 by AZD4547 also prevented a decrease in *miR-221* and *miR-222* and the synthetic phenotype induced by FGF23. VSMCs incubated with FGF23 recovered the contractile phenotype after the inhibition of Erk1/2 phosphorylation with PD98059. *miR-221* and *miR-222* transfections decreased MAP3K2 and PAK1 expressions as well as Erk1/2 phosphorylation, which promoted a contractile phenotype.

In experimental animals, a constant infusion of recombinant FGF23 decreased aortic levels of *miR-221* with a concomitant increase in arterial stiffness. In these rats, a remarkable change was observed in VSMC morphology, with a significant increase in aortic wall thickness and decreased expression of elastin protein and synthetic markers of VSMCs.

The reduction in the contractile feature of VSMCs in favour of the synthetic phenotype has haemodynamic consequences. These preclinical results prompted us to analyse a possible association between FGF23 levels and peripheral PP in patients with CKD stage 2–3. It was observed that C-FGF23 was positively correlated with parameters of arterial stiffening (PP and PWV). Furthermore, the plasma concentrations of *miR-221* and *miR-222* were significantly reduced in patients with the highest level of FGF23.

A direct interaction of FGF23 with FGFR1 has been described in other cell types such as chondrocytes or osteoblast cells, even in the absence of Klotho [33]. It has been shown that FGF23, through its action on FGFR, phosphorylates Erk1/2 in VSMCs [34] and other types of cells [35, 36]. MAP3K2, a target gene of *miR-221/222*, has been recently associated with an aberrant Erk1/2 activation in neurofibromatosis type 1 [37]. In addition, PAK1 protein, another target of *miR-221*, also favours Erk1/2 phosphorylation [38], while an increased expression of *miR-221* inhibits PAK1 expression, which impairs Erk1/2 phosphorylation [39]. Therefore the reduction of *miR-221/222* induced by FGF23 may promote Erk1/2 phosphorylation via two different mechanisms, the upregulation of MAP3K2 and PAK1.

A new finding obtained in the present study is the reduction of miRNA biogenesis in VSMCs induced by high levels of FGF23. The mechanisms whereby FGF23 decreases miRNA biogenesis are not completely defined. It has been observed that activated Erk may cause widespread miRNA repression by suppressing major steps of miRNA biogenesis [40]. In liver cancer, Erk phosphorylation suppresses pre-miRNA export from the nucleus through phosphorylation of *exportin 5* [41]. Therefore excessive Erk1/2 phosphorylation induced by high levels of FGF23 could be responsible for the reduction in miRNA biogenesis.

There is evidence that *miR-221/222* are involved in the regulation of essential vascular processes such as angiogenesis [42], neointimal hyperplasia [43], vessel wound healing [44], vascular aging [45] and atherosclerotic vascular remodelling [46]. In advanced atherosclerosis, associated with long-term chronic inflammation and remodelling of the intima, *miR-221/222* is downregulated in vascular endothelial cells [19]. Other reports have shown reduced serum *miR-221* levels in subjects with atherosclerosis obliterans and atherosclerotic patients with subclinical hypothyroidism [47, 48]. Conversely, other investigators have shown elevated levels of *miR-221* in serum from patients with metabolic syndrome [49]. It would be relevant to know if, in patients with metabolic syndrome, the decline in renal function with the concomitant increase in FGF23 is associated with a reduction of *miR-221*, arterial stiffening and vascular dysfunction. Regarding the relationship between *miR-221* and the phenotypic switching of VSMCs, the published results available are not uniform. Davis *et al.* [20] showed that in VSMCs, upregulation of *miR-221* after incubation with platelet-derived growth factor (PDGF) for 24 hours promotes a synthetic phenotype of VSMCs. Of interest, the downregulation of *miR-221* has been associated with the development of an osteogenic phenotype in VSMCs. Mackenzie *et al.* [50] showed that in VSMCs, high phosphate levels produced a downregulation of *miR-221* and calcification; a possible interpretation of these results is that the response to *miR-221* may be time dependent. Studies on

human stem cells show that *miR-222* is upregulated during the initiation of differentiation to neuronal cells and was subsequently reduced as the cells reached full differentiation [51]. Another potential explanation could be that vascular compliance, and therefore the functional demand of VSMCs in different arteries, should not be the same. In arteries such as the carotid [18] or pulmonary arteries [20], the vascular tone and elasticity are different than in the aorta. Thus a pro-synthetic effect of elevated *miR-221* may not be comparable in all VSMCs. Davis *et al.* [20] showed that administration of PDGF to pulmonary VSMCs increased *miR-221*, promoting the synthetic phenotype of these cells. Certainly more studies in these cells are warranted to define the specific effects of miRNA.

The finding of a direct effect of FGF23 on both *miR-221* and *miR-222* is based on *in vitro* and *in vivo* experiments and the key role of these miRNAs on the VSMC phenotype is illustrated by the fact that in VSMCs transfected with *miR-221*, FGF23 failed to induce a synthetic phenotype. The specific mechanism whereby FGF23 downregulates *miR-221/222* is not known. Several hypotheses may be proposed; in aortic VSMCs, the downregulation of *miR-221* induced by FGF23 might be explained by the participation of oestrogen receptors. Oestrogen receptors are known to be negative modulators of *miR-221/222* and cluster through the recruitment of transcriptional corepressor partners: nuclear receptor corepressor and silencing mediator of retinoic acid and thyroid hormone receptor [32]. In addition, it has been demonstrated that oestradiol increases arterial stiffness [52] and the synthetic phenotype of aortic VSMCs [53], likely through downregulation of *miR-221*.

Another potential mechanism involved may be related to the effect of endoplasmic reticulum (ER) stress on *miR-221/222* expression. It has been observed that during ER stress, there is a downregulation of *miR-221/222* [54]. Activation of mammalian target of rapamycin (mTOR) induces ER stress [55] and our group has shown that FGF23 produces mTOR activation [56]. Other authors have also explored the effect of mTOR activation on phenotypic switching of VSMCs [57]. Therefore it is possible that FGF23 causes mTOR activation, which in turn promotes ER stress with the subsequent downregulation of *miR-221/222*.

Another potential mechanism may be the participation of the long non-coding RNA KCNQ1OT1, which through its interaction with *miR-221* may affect migration, proliferation, inflammation and hyperplasia of VSMCs [58]. It has been shown that β-catenin can stimulate KCNQ1OT1 transcription through direct binding to the KCNQ1OT1 promoter [59]. There is evidence that FGF23 can induce nuclear translocation of β-catenin [60]. Thus FGF23, through β-catenin, may increase long non-coding RNA KCNQ1OT1 expression and the downregulation of *miR-221*, leading to changes in the VSMC phenotype and arterial stiffening of the aorta.

Our study is the first to describe that FGF23 promotes the phenotypic transition of VSMCs from contractile to synthetic. This change in VSMCs could explain the different responses of arterial rings from FGF23-treated animals in response to 70K and noradrenaline. The stretch–force relationship exhibited by arterial rings indicated that as compared with controls, arteries from rats treated with FGF23 required less stretch to reach 100 mmHg of transmural pressure. The stress–strain relationship was also measured to determine if resistance could be due to increased material stiffness. Rings from FGF23-treated rats showed a high stress–strain relation, which is a similar finding to that observed in other animal models of increased vascular stiffness [61]. Six *et al.* [62] observed an acute effect of FGF23 on mouse aortic ring constriction, although only with fairly high concentrations of FGF23 (400 ng/ml), and no constriction effect was observed with lower concentrations of FGF23, as was observed in our experiment. Certainly the addition of klotho partially reverted the vasoconstriction induced by high concentrations of FGF23 via increased nitric oxide production.

These results suggest that FGF23 makes the thoracic aorta more resistant to distension as a result of increased arterial stiffness. Consistent with this change is the decreased active wall tension, or force exerted by a vessel wall during VSMC contraction, observed in FGF23-treated animals. Since PWV is related to the intrinsic elastic properties as well as to the arterial geometry and the applied BP, the increase observed in PWV in CKD patients is likely explained by a reduction in the distensibility of arteries as a consequence of increased stiffness. The increased arterial stiffness observed under pathological conditions could facilitate early wave reflection, amplifying systolic and reducing diastolic aortic pressure, with the consequent increase in PP [63]. These changes could also be related to the histological modifications observed in thoracic aortas of FGF23-treated rats. Changes in the nuclear orientation of VSMCs and tunica media thickness could be a consequence of the phenotypic transition of VSMCs, leading to increased arterial stiffness. This change in the orientation of nuclei was observed in VSMCs with a synthetic phenotype from aortas of patients with aortopathy associated with valve stenosis [64], suggesting that this change in VSMC morphology could be a response to haemodynamic factors or tensile strains.

An excessive predominance of the VSMC synthetic phenotype induced by FGF23 may cause arterial stiffness. PWV and peripheral PP are markers of arterial stiffening [65]. In a limited group of CKD stage 2–3 patients, the concentration of C-FGF23 correlated with peripheral and central PP, independent of the eGFR. Therefore high FGF23 levels may favour stiffness in vessels through the transition of VSMCs from a contractile to a synthetic phenotype. The reduction of *miR-221* and *miR-222* in patients with the highest C-FGF23 supports the notion that high C-FGF23 levels favour the transition of VSMCs to the synthetic phenotype. Many studies have shown an association between elevated FGF23 and negative cardiovascular outcomes in patients with and without CKD [66]. This has been explained by the fact that FGF23 is mainly responsible for the development of left ventricular hypertrophy [5]; the present study suggests that the direct effect of FGF23 on the vascular wall may also contribute to an increase cardiovascular mortality.

With respect to the potential effects of FGF23 on the vasculature, there are other additional aspects that should be mentioned, such as its potential involvement on vascular calcification and the effect of klotho. Jimbo *et al.* [34]

demonstrated that in aortic rings, the addition of recombinant FGF23 (10 ng/ml) for 6 days increased phosphate-induced vascular calcification. These effects were mediated by FGFR1 and ERK1/2 phosphorylation, and the presence of klotho did not prevent this effect. In this sense, in patients with CKD stage 4–5 versus healthy controls, Krishnasamy *et al.* [67] found a significant association between serum FGF23 and arterial calcification and stiffness. However, Scialla *et al.* [68] observed that FGF23 did not modify the osteogenic phenotype of VSMCs. They demonstrated that FGF23 was not associated with arterial calcification in patients and did not promote calcification *in vitro*; also, they observed that FGF23 (with and without the presence of soluble klotho) does not affect VSMC phosphate uptake. Linderberg *et al.* [69] observed that FGF23 in concentrations of 0.125–2 ng/ml, and in the absence of vascular Klotho, does not modify calcification in bovine VSMCs, and in arterial specimens of mice *ex vivo*, it did not affect dilatory, contractile and structural properties. It seems that more studies are necessary to elucidate the role of FGF23 on vascular calcification.

With respect to the role of klotho, the presence or absence of α-klotho at a vascular level has been studied by several authors [69, 70]. Some investigators propose that part of the associated complication derived from high levels of FGF23 is due to klotho deficiency [71, 72]. Our data show that human aortic VSMCs do not express transmembrane klotho, however, a band of 70 kDa was detected that would correspond with soluble klotho; this band was not modified by the addition of FGF23 to human VSMCs in culture (data not shown). Additionally, co-administration of FGF23 and recombinant klotho to VSMCs did not modify the decreased expression of contractile markers of VSMCs induced by FGF23 (Supplementary material, Figure S2). It can be speculated that vascular klotho deficiency by aging or CKD might be one of the causes of VSMC phenotypic switching induced by FGF23. However, our results suggest that the presence of klotho does not prevent the effects of FGF23 on phenotypic switching of VSMCs.

In summary, FGF23 causes the transition of VSMCs from a contractile to a synthetic phenotype, producing an increase in vascular stiffness and alteration of the biomechanical properties of the arteries. This may be a mechanism by which FGF23 contributes directly to the development of vascular dysfunction and cardiovascular mortality in CKD patients. This finding opens up new perspectives for treatment of vascular diseases that is specific for CKD, where marked increases in serum FGF23 are manifested almost universally.

SUPPLEMENTARY DATA

Supplementary data is available at *ndt* online.

ACKNOWLEDGEMENTS

We thank Gema Garcia Jurado, from the Maimonides Institute for Biomedical Research of Cordoba Facility of Microscopy, for the acquisition of the confocal images.

FUNDING

This work was supported by a Spanish government grant from the Programa Nacional I+D+I 2013–2016 and Instituto de Salud Carlos III (ISCIII) grants PI18/0138 and PI21/0654 co-financing from European Funds (FEDER), Consejería de Salud (grants PI-0136 and PI-0169-2020) from the Junta de Andalucía, Framework Programme 7 Syskid UE grant FP7-241544, and EUTOX and REDinREN from the ISCIII. N.V. and J.M.D.-T. were supported by Consejería de Economía, Innovación, Ciencia y Empleo (grant CVI-7925) from the Junta de Andalucía. Y.A. and J.R.M.-C. are senior researchers supported by the Nicolás Monardes Programme, Consejería de Salud-Servicio Andaluz de Salud (Junta de Andalucía).

AUTHORS' CONTRIBUTIONS

N.V., M.V.P.-R.d.M. and C.R.-H. were responsible for the methodology, validation, investigation, resources, formal analysis and original draft.

G.R.-G., C.M., J.M.D.-T., J.M.M.-M., A.T., C.H., M.R.-O. and R.L.-B. were responsible for the methodology, validation and investigation.

R.S. was responsible for the formal analysis and review and editing.

J.U., W.G.R., A.F., Y.A. and A.M.-M. were responsible for review and editing. S.S. was responsible for supervision and project administration.

M.R. was responsible for conceptualization, methodology, review and editing, resources, supervision and project administration. J.R.M.-C. was responsible for conceptualization, methodology and review editing, validation, resources, formal analysis, visualization and funding acquisition.

DATA AVAILABILITY STATEMENT

The data underlying this article will be shared on reasonable request to the corresponding author.

CONFLICT OF INTEREST STATEMENT

R.W.G. was employed by Amgen. M.R. has received honorarium for lectures from Amgen, Fresenius, Viphor and Kyowa. The remaining authors declare no conflicts of interest.

REFERENCES

1. Shimada T, Hasegawa H, Yamazaki Y *et al.* FGF-23 is a potent regulator of vitamin D metabolism and phosphate homeostasis. *J Bone Miner Res* 2004;**19**:429–35.
2. Ben-Dov IZ, Galitzer H, Lavi-Moshayoff V *et al.* The parathyroid is a target organ for FGF23 in rats. *J Clin Invest* 2007;**117**:4003–8.
3. Kuczera P, Adamczak M, Wiecek A. Fibroblast growth factor-23—a potential uremic toxin. *Toxins* 2016;**8**:369.
4. Jialal I, Camacho F, Nathoo B *et al.* Fibroblast growth factor 23 predicts mortality and end-stage renal disease in a Canadian Asian population with chronic kidney disease. *Nephron* 2017;**137**:190–6.
5. Faul C, Amaral AP, Oskouei B *et al.* FGF23 induces left ventricular hypertrophy. *J Clin Invest* 2011;**121**:4393–408.
6. Grabner A, Amaral AP, Schramm K *et al.* Activation of cardiac fibroblast growth factor receptor 4 causes left ventricular hypertrophy. *Cell Metab* 2015;**22**:1020–32.

7. Silswal N, Touchberry CD, Daniel DR *et al.* FGF23 directly impairs endothelium-dependent vasorelaxation by increasing superoxide levels and reducing nitric oxide bioavailability. *Am J Physiol Endocrinol Metab* 2014;**307**:E426–36.
8. Verkaik M, Juni RP, van Loon EPM *et al.* FGF23 impairs peripheral microvascular function in renal failure. *Am J Physiol Heart Circ Physiol* 2018;**315**:H1414–24.
9. Rensen SSM, Doevendans PAFM, van Eys GJJM. Regulation and characteristics of vascular smooth muscle cell phenotypic diversity. *Neth Heart J* 2007;**15**:100–8.
10. Bacakova L, Travnickova M, Filova E *et al.* The role of vascular smooth muscle cells in the physiology and pathophysiology of blood vessels. IntechOpen, 2018. https://www.intechopen.com/chapters/61602 (16 February 2022, date last accessed).
11. Frismantiene A, Philippova M, Erne P *et al.* Smooth muscle cell-driven vascular diseases and molecular mechanisms of VSMC plasticity. *Cell Signalling* 2018;**52**:48–64.
12. Schachter M. Vascular smooth muscle cell migration, atherosclerosis, and calcium channel blockers. *Int J Cardiol* 1997;**62**(Suppl 2):S85–90.
13. Karnik SK, Brooke BS, Bayes-Genis A *et al.* A critical role for elastin signaling in vascular morphogenesis and disease. *Development* 2003;**130**:411–23.
14. Shanahan CM, Weissberg PL. Smooth muscle cell heterogeneity: patterns of gene expression in vascular smooth muscle cells in vitro and in vivo. *Arterioscler Thromb Vasc Biol* 1998;**18**:333–8.
15. Owens GK, Kumar MS, Wamhoff BR. Molecular regulation of vascular smooth muscle cell differentiation in development and disease. *Physiol Rev* 2004;**84**:767–801.
16. Cocciolone AJ, Hawes JZ, Staiculescu MC *et al.* Elastin, arterial mechanics, and cardiovascular disease. *Am J Physiol Heart Circ Physiol* 2018;**315**:H189–205.
17. Zhang C. Novel functions for small RNA molecules. *Curr Opin Mol Ther* 2009;**11**:641–51.
18. Liu X, Cheng Y, Yang J *et al.* Cell-specific effects of miR-221/222 in vessels: molecular mechanism and therapeutic application. *J Mol Cell Cardiol* 2012;**52**:245–55.
19. Chistiakov DA, Sobenin IA, Orekhov AN *et al.* Human miR-221/222 in physiological and atherosclerotic vascular remodeling. *Biomed Res Int* 2015;**2015**:354517.
20. Davis BN, Hilyard AC, Nguyen PH *et al.* Induction of microRNA-221 by platelet-derived growth factor signaling is critical for modulation of vascular smooth muscle phenotype. *J Biol Chem* 2009;**284**:3728–38.
21. Mori-Abe A, Tsutsumi S, Takahashi K *et al.* Estrogen and raloxifene induce apoptosis by activating p38 mitogen-activated protein kinase cascade in synthetic vascular smooth muscle cells. *J Endocrinol* 2003;**178**:417–26.
22. Muñoz-Castañeda JR, Herencia C, Pendón-Ruiz de Mier MV *et al.* Differential regulation of renal klotho and FGFR1 in normal and uremic rats. *FASEB J* 2017;**31**:3858–67.
23. Vogel B, Siebert H, Hofmann U *et al.* Determination of collagen content within picrosirius red stained paraffin-embedded tissue sections using fluorescence microscopy. *MethodsX* 2015;**2**:124–34.
24. Cox RH. Comparison of mechanical and chemical properties of extra- and intralobar canine pulmonary arteries. *Am J Physiol* 1982;**242**:H245–53.
25. Alberti KGMM, Eckel RH, Grundy SM *et al.* Harmonizing the metabolic syndrome: a joint interim statement of the International Diabetes Federation Task Force on Epidemiology and Prevention; National Heart, Lung, and Blood Institute; American Heart Association; World Heart Federation; International Atherosclerosis Society; and International Association for the Study of Obesity. *Circulation* 2009;**120**:1640–5.
26. Weiss W, Gohlisch C, Harsch-Gladisch C *et al.* Oscillometric estimation of central blood pressure: validation of the Mobil-O-Graph in comparison with the SphygmoCor device. *Blood Press Monit* 2012;**17**:128–31.
27. Reference Values for Arterial Stiffness' Collaboration. Determinants of pulse wave velocity in healthy people and in the presence of cardiovascular risk factors: 'establishing normal and reference values'. *Eur Heart J* 2010;**31**:2338–50.
28. Ashraf JV, Al Haj Zen A. Role of vascular smooth muscle cell phenotype switching in arteriogenesis. *Int J Mol Sci* 2021;**22**:10585.
29. Shi J, Yang Y, Cheng A *et al.* Metabolism of vascular smooth muscle cells in vascular diseases. *Am J Physiol Heart Circ Physiol* 2020;**319**:H613–31.
30. Nanoudis S, Pikilidou M, Yavropoulou M *et al.* The role of microRNAs in arterial stiffness and arterial calcification. An update and review of the literature. *Front Genet* 2017;**8**:209.
31. Jin W, Reddy MA, Chen Z *et al.* Small RNA sequencing reveals microRNAs that modulate angiotensin II effects in vascular smooth muscle cells. *J Biol Chem* 2012;**287**:15672–83.
32. Di Leva G, Gasparini P, Piovan C *et al.* MicroRNA cluster 221-222 and estrogen receptor α interactions in breast cancer. *J Natl Cancer Inst* 2010;**102**:706–21.
33. Bianchi A, Guibert M, Cailotto F *et al.* Fibroblast growth factor 23 drives MMP13 expression in human osteoarthritic chondrocytes in a klotho-independent manner. *Osteoarthritis Cartilage* 2016;**24**:1961–9.
34. Jimbo R, Kawakami-Mori F, Mu S *et al.* Fibroblast growth factor 23 accelerates phosphate-induced vascular calcification in the absence of klotho deficiency. *Kidney Int* 2014;**85**:1103–11.
35. Kyono A, Avishai N, Ouyang Z *et al.* FGF and ERK signaling coordinately regulate mineralization-related genes and play essential roles in osteocyte differentiation. *J Bone Miner Metab* 2012;**30**:19–30.
36. Canalejo R, Canalejo A, Martinez-Moreno JM *et al.* FGF23 fails to inhibit uremic parathyroid glands. *J Am Soc Nephrol* 2010;**21**:1125–35.
37. Bok S, Shin DY, Yallowitz AR *et al.* MEKK2 mediates aberrant ERK activation in neurofibromatosis type I. *Nat Commun* 2020;**11**:5704.
38. Shrestha Y, Schafer EJ, Boehm JS *et al.* PAK1 is a breast cancer oncogene that coordinately activates MAPK and MET signaling. *Oncogene* 2012;**31**:3397–408.
39. Zhang X, Mao H, Chen J *et al.* Increased expression of microRNA-221 inhibits PAK1 in endothelial progenitor cells and impairs its function via c-Raf/MEK/ERK pathway. *Biochem Biophys Res Commun* 2013;**431**:404–8.
40. Qu Y, Shi B, Hou P. Activated ERK: an emerging player in miRNA downregulation. *Trends Cancer* 2017;**3**:163–5.
41. Sun H-L, Cui R, Zhou J *et al.* ERK activation globally downregulates miRNAs through phosphorylating exportin-5. *Cancer Cell* 2016;**30**:723–36.
42. Kuehbacher A, Urbich C, Dimmeler S. Targeting microRNA expression to regulate angiogenesis. *Trends Pharmacol Sci* 2008;**29**:12–5.
43. Albinsson S, Sessa WC. Can microRNAs control vascular smooth muscle phenotypic modulation and the response to injury? *Physiol Genomics* 2011;**43**:529–33.
44. Song Z, Li G. Role of specific microRNAs in regulation of vascular smooth muscle cell differentiation and the response to injury. *J Cardiovasc Transl Res* 2010;**3**:246–50.
45. Rippe C, Blimline M, Magerko KA *et al.* MicroRNA changes in human arterial endothelial cells with senescence: relation to apoptosis, eNOS and inflammation. *Exp Gerontol* 2012;**47**:45–51.
46. Bazan HA, Hatfield SA, O'Malley CB *et al.* Acute loss of miR-221 and miR-222 in the atherosclerotic plaque shoulder accompanies plaque rupture. *Stroke* 2015;**46**:3285–7.
47. Li T, Cao H, Zhuang J *et al.* Identification of miR-130a, miR-27b and miR-210 as serum biomarkers for atherosclerosis obliterans. *Clin Chim Acta* 2011;**412**:66–70.
48. Zhang X, Shao S, Geng H *et al.* Expression profiles of six circulating microRNAs critical to atherosclerosis in patients with subclinical hypothyroidism: a clinical study. *J Clin Endocrinol Metab* 2014;**99**:E766–74.
49. Wang Y-T, Tsai P-C, Liao Y-C *et al.* Circulating microRNAs have a sex-specific association with metabolic syndrome. *J Biomed Sci* 2013;**20**:72.
50. Mackenzie NCW, Staines KA, Zhu D *et al.* miRNA-221 and miRNA-222 synergistically function to promote vascular calcification. *Cell Biochem Funct* 2014;**32**:209–16.
51. Wu H, Xu J, Pang ZP *et al.* Integrative genomic and functional analyses reveal neuronal subtype differentiation bias in human embryonic stem cell lines. *Proc Natl Acad Sci USA* 2007;**104**:13821–6.
52. Tatchum-Talom R, Martel C, Marette A. Influence of estrogen on aortic stiffness and endothelial function in female rats. *Am J Physiol Heart Circ Physiol* 2002;**282**:H491–8.
53. Zha B, Qiu P, Zhang C *et al.* GPR30 promotes the phenotypic switching of vascular smooth muscle cells via activating the AKT and ERK pathways. *Onco Targets Ther* 2020;**13**:3801–8.
54. Dai R, Li J, Liu Y *et al.* miR-221/222 suppression protects against endoplasmic reticulum stress-induced apoptosis via p27(Kip1)-

and MEK/ERK-mediated cell cycle regulation. *Biol Chem* 2010;**391**: 791–801.
55. Panda DK, Bai X, Sabbagh Y *et al.* Defective interplay between mTORC1 activity and endoplasmic reticulum stress-unfolded protein response in uremic vascular calcification. *Am J Physiol Renal Physiol* 2018;**314**: F1046–61.
56. Vidal A, Rios R, Pineda C *et al.* Direct regulation of fibroblast growth factor 23 by energy intake through mTOR. *Sci Rep* 2020;**10**:1795.
57. Ni T, Gao F, Zhang J *et al.* Impaired autophagy mediates hyperhomocysteinemia-induced HA-VSMC phenotypic switching. *J Mol Histol* 2019;**50**:305–14.
58. Ye B, Wu Z-H, Tsui TY *et al.* lncRNA KCNQ1OT1 suppresses the inflammation and proliferation of vascular smooth muscle cells through IκBa in intimal hyperplasia. *Mol Ther Nucleic Acids* 2020;**20**:62–72.
59. Sunamura N, Ohira T, Kataoka M *et al.* Regulation of functional KCNQ1OT1 lncRNA by β-catenin. *Sci Rep* 2016;**6**:20690.
60. Meo Burt P, Xiao L, Hurley MM. FGF23 regulates Wnt/β-catenin signaling-mediated osteoarthritis in mice overexpressing high-molecular-weight FGF2. *Endocrinology* 2018;**159**:2386–96.
61. Resch M, Schmid P, Amann K *et al.* Eplerenone prevents salt-induced vascular stiffness in Zucker diabetic fatty rats: a preliminary report. *Cardiovasc Diabetol* 2011;**10**:94.
62. Six I, Okazaki H, Gross P *et al.* Direct, acute effects of klotho and FGF23 on vascular smooth muscle and endothelium. *PLoS One* 2014;**9**: e93423.
63. Briet M, Boutouyrie P, Laurent S *et al.* Arterial stiffness and pulse pressure in CKD and ESRD. *Kidney Int* 2012;**82**:388–400.
64. Forte A, Della Corte A, Grossi M *et al.* Early cell changes and TGFβ pathway alterations in the aortopathy associated with bicuspid aortic valve stenosis. *Clin Sci (Lond)* 2013;**124**:97–108.
65. Laurent S, Cockcroft J, Van Bortel L *et al.* Expert consensus document on arterial stiffness: methodological issues and clinical applications. *Eur Heart J* 2006;**27**:2588–605.
66. Souma N, Isakova T, Lipiszko D *et al.* Fibroblast growth factor 23 and cause-specific mortality in the general population: the Northern Manhattan Study. *J Clin Endocrinol Metab* 2016;**101**:3779–86.
67. Krishnasamy R, Tan S-J, Hawley CM *et al.* Progression of arterial stiffness is associated with changes in bone mineral markers in advanced CKD. *BMC Nephrol* 2017;**18**:281.
68. Scialla JJ, Lau WL, Reilly MP *et al.* Fibroblast growth factor 23 is not associated with and does not induce arterial calcification. *Kidney Int* 2013;**83**:1159–68.
69. Lindberg K, Olauson H, Amin R *et al.* Arterial klotho expression and FGF23 effects on vascular calcification and function. *PLoS One* 2013;**8**:e60658.
70. Lim K, Lu T-S, Molostvov G *et al.* Vascular klotho deficiency potentiates the development of human artery calcification and mediates resistance to fibroblast growth factor 23. *Circulation* 2012;**125**:2243–55.
71. Hénaut L, Mary A, Chillon J-M *et al.* The impact of uremic toxins on vascular smooth muscle cell function. *Toxins* 2018;**10**:218.
72. Hu MC, Shi M, Zhang J *et al.* Klotho deficiency causes vascular calcification in chronic kidney disease. *J Am Soc Nephrol* 2011;**22**:124–36.

Received: 21.2.2022; Editorial decision: 22.6.2022